Performability Evaluation of Water Distribution Systems During Maintenance Procedures

Laura Carnevali, Fabio Tarani, and Enrico Vicario, *Member, IEEE*

***Abstract*—A Water Distribution System (WDS) is a critical infrastructure for society and economy, subject to frequent maintenance either for contingencies or planned operations. Maintenance procedures affect the hybrid dynamics of a WDS at stochastic time points, representing the completion of repair activities that change the WDS topology and operation mode. Hence, the problem of performability evaluation of the WDS behavior during a maintenance intervention falls in the class of stochastic hybrid systems (SHSs), for which existing numerical or simulative approaches cannot afford the complexity of realistic WDSs. We propose a viable approach that computes the expected demand not served during a maintenance procedure by integrating fluid-dynamic analysis of the WDS with quantitative evaluation of the procedure timing, notably assuming non-Markovian repair times over a bounded support. Different solution techniques are presented to evaluate the joint distribution of the times when the procedure affects the WDS, performing either simulation of the procedure model or state-space analysis based on an extension of the method of stochastic state classes. Feasibility and effectiveness of the proposed methods are assessed on a real WDS in terms of result accuracy and computational complexity, showing that the overall approach could be efficiently applied in higher level tasks including activity scheduling, resource planning, and budget allocation.**

***Index Terms*—Demand Not Served (DNS), maintenance procedure, performability evaluation, Stochastic Hybrid System (SHS), stochastic state class, Water Distribution System (WDS).**

I. Introduction

A WATER Distribution System (WDS) is a networked hydraulic control infrastructure, designed to convey water from sources to treatment plants up to water mains supplying end users [1], [2]. Water distribution is an essential facility not only to safeguard vital societal functions and public health, but also to guarantee correct operation of other interdependent systems, including emergency services, food production, and manufacturing, with consequent significant impact on safety, economy, and environment. To increase system availability and avoid outages in water delivery, redundancy is usually implemented by incorporating additional pumps, backup power generators, and extra tanks. Nevertheless, interruption or reduction in service may be experienced during maintenance of water mains, which occurs quite frequently in practice, due to either contingencies or planned activities. In both cases, quantitative evaluation of the level of disruption experienced by consumers during maintenance procedures becomes relevant for operation planning, budget allocation, and qualification of service operators, especially in the emergent context of open-market policies and privatization of public waterworks.

The problem couples some major factors of complexity. On one hand, a WDS is inherently a *hybrid system*, with water flow determined by deterministic nonlinear differential equations on nodal pressures, pipe flow rates, and water level in tanks (*continuous dynamics*), as well as by the operation mode of various components, notably pumps and valves, which in turn results from a deterministic control policy possibly depending on nodal pressures and absolute time of day (*discrete dynamics*). On the other hand, during maintenance, topology and operation mode of the network can be changed at stochastic time points corresponding to the completion of intermediate actions in the repair procedure and resulting from the combination of multiple activities with stochastic duration, usually non-Markovian and supported within a bounded deadline by contract or by necessity. The two complexities together cast the problem in the class of Stochastic Hybrid Systems (SHSs) [3].

Several classes of SHSs have been introduced to account for probabilistic uncertainty in a hybrid dynamics, not specifically related to WDSs. In [4], verification of a discrete-time SHS is performed through model checking of an approximating discrete-time Markov chain, providing guarantees on the attained approximation level. Optimal control problems are investigated in [5] for piece-wise deterministic Markov processes, which combine (continuous-time) random discrete jumps with a deterministic continuous evolution characterized by ordinary differential equations. The approach is extended in [6] to general SHSs, letting the evolution of continuous variables between two consecutive jumps be a diffusion process. In [7], Monte-Carlo simulation of a discrete-time SHS is performed using an exact Bayesian filter estimated from conditional mode probabilities given the observations. A model checking technique is applied in [8] for correctness verification of systems that include both a discrete logic, represented by a Markov chain, and a stochastic dynamics, accounted by a set of stochastic differential equations. Verification of reachability properties of SHSs is also addressed in [9] by numerically

Manuscript received September 26, 2016; revised May 9, 2017 and August 2, 2017; accepted November 28, 2017. Date of publication February 16, 2018; date of current version April 15, 2020. This paper was recommended by Associate Editor K. W. Hipel. *(Corresponding author: Laura Carnevali.)*

The authors are with the Department of Information Engineering, University of Florence, 50139 Florence, Italy (e-mail: laura.carnevali@unifi.it; fabio.tarani@unifi.it; enrico.vicario@unifi.it).

Color versions of one or more of the figures in this paper are available online at http://ieeexplore.ieee.org.

Digital Object Identifier 10.1109/TSMC.2017.2783188

solving a system of partial differential equations. As a common trait, in all these approaches memory of continuous variables is lost upon discrete mode transitions, preventing the representation of times of day, which influence both consumption patterns and operation scheduling, and durations with a nonmemoryless distribution. Moreover, general numerical solution techniques for the quantitative evaluation of SHSs are not able to afford the actual complexity of realistic WDSs.

Fluid stochastic Petri nets [10] support the representation of continuous variables, accounted by fluid places holding a real-valued amount of fluid, as well as random events, modeled through discrete places containing a natural number of tokens. In principle, the formalism is amenable to numerical solution under fairly strong assumptions on the interaction between continuous and discrete dynamics, both for exponentially distributed [11], [12] and general transitions [13]; in practice, simulation turns out to be the only viable approach for models with more than two continuous variables [14]. Hybrid Petri nets overcome the limit by allowing an arbitrary number of continuous places, provided that a single generally distributed transition is allowed and with only one firing [15]. The solution technique is applied in [16] to evaluate the survivability of a sewage treatment facility under variable weather conditions, using the general transition to model the distribution of rain duration. In [17], the approach is extended to the case of two concurrently enabled general transitions, but the structure of the Petri model directly reflects the WDS network topology, which comprises a major limit in the representation of a WDS. Fluidization of transitions is applied in [18] to avoid state-space explosion, though referring to Petri net models that satisfy the Markovian assumption.

In [19], quantitative evaluation of the impact of a repair procedure is proposed for the case of a gas distribution network, which is a similar problem in the application perspective, but develops on much different underlying mathematics: in a gas distribution network, pressure applied at input nodes can be controlled independently of the state and history of the network; conversely, in water distribution, node pressure depends on the filling level of tanks, which in turn depends on the past continuous history of incoming fluxes and served demand. Moreover, the behavior of active components of a WDS, such as pumps, may depend on continuous state variables, notably on node pressures or tank levels, and the system may not attend a steady state, even if the boundary conditions in terms of nodal demands are constant.

In this paper, we evaluate the WDS performability during a maintenance procedure through the expected Demand Not Served (DNS) over time, taking into account water consumption varying with the time of day according to several load patterns, non-Markovian repair times bounded by contractual constraints, and daily work schedules depending on the criticality level of repair operations. To this end, we derive a stochastic model of the procedure from a UML-based specification, introducing dynamic Stochastic Time Petri Nets (dynamic-sTPNs) which include clocks supporting evaluation of the time spent in each WDS topology; then, we evaluate the joint domain and distribution of the stochastic times when the procedure affects the WDS behavior, leveraging simulation of the procedure model or analysis based on an extension of the method of stochastic state classes [20], [21]; finally, we perform fluid-dynamic analysis of the WDS subordinated to each obtained time point, weighting rewards according to point probabilities. The analytical solution allows a significant reduction in the number of fluid-dynamic analyses in the case that all users are properly served as soon as repair is over and the WDS topology is restored; moreover, the extension of the method of stochastic state classes with clock variables comprises a theoretical contribution beyond the scope of this paper. The approach is experimented on a real WDS, studied in the literature on optimization of WDS operation [22], [23], evaluating accuracy and complexity of the proposed solution methods. Experimental results show that the simulative approach achieves the best tradeoff between accuracy and complexity when a coarse-grained precision is sufficient or the procedure complexity is exacerbated; conversely, the analytical solution becomes more convenient when a fine-grained accuracy is required or the WDS complexity is significantly increased. In the applicative perspective, the computed performability measures open the way to various objectives, including optimization of maintenance interventions, allocation of budget to increase the WDS resilience, and quantitative evaluation of the effects of failures, especially in combination with statistical information on breakdowns of components.

The rest of this paper is organized in five sections. In Section II, we formulate the problem (Sections II-A and II-B) and present the salient traits of the approach (Section II-C). In Section III, we present syntax and semantics of dynamic-sTPNs (Section III-A), we derive a dynamic-sTPN model of the maintenance procedure (Section III-B), we extend the method of stochastic state classes with clock variables (Section III-C), and we sample the symbolic form of the joint distribution of the stochastic times when the procedure affects the WDS behavior (Section III-D). In Section IV, we discuss fluid-dynamic analysis of the WDS (Section IV-A) and evaluate the expected DNS over time through different solution methods (Section IV-B). In Section V, we discuss the experimental setup (Section V-A) and the obtained results (Section V-B). Conclusions are drawn in Section VI. For the sake of readability, technical details on the extension of the method of stochastic state classes are reported in the Appendix.

II. Problem Formulation and Solution Approach

A. Water Distribution Systems

Water distribution infrastructures deliver water from a natural source or treatment facility to end users. Contractual constraints regulate the flow rate to be supplied and the pressure at the user-network interface, which must be controlled between a minimum defined by quality standards and a maximum limited by mechanical properties of network components and user appliances; additional nonfunctional requirements for operators are network dependability and robustness, minimization of water leaks, and economy of operation related to pump power consumption and maintenance costs. Water is displaced by various types of components, including pipes, pumps, valves,

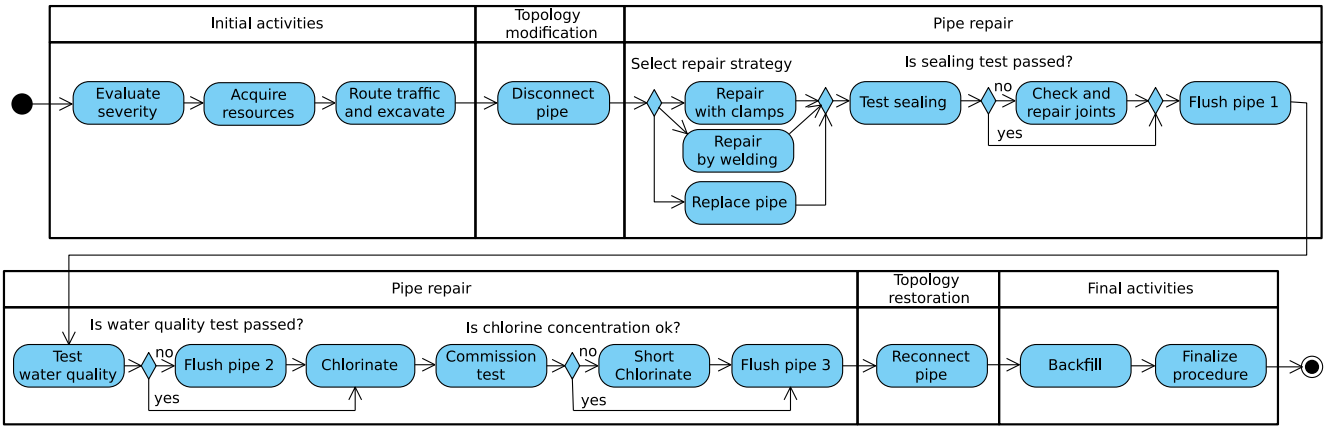

Fig. 1. UML activity diagram of a five-phase maintenance procedure for the repair of a failed pipe.

and controls, as well as fittings, fire hydrants, and blow-offs; water can also be stored in tanks to enhance reliability and efficiency by decoupling production. The assembly of all these components is referred to as WDS [1].

The piping is classified into either *transmission* mains, conveying large amounts of water over great distances, or *distribution* mains, smaller in diameter and used to deliver water from transmission mains to users. Transmission mains usually feature a branched topology, given that size and cost of pipes make redundancy not cost-effective, whereas distribution mains tend to follow street alignment and are densely looped; a variety of fittings (e.g., elbows, tees, etc.) is needed to accommodate the piping topology. Pumps are used to provide water with the energy needed to overcome height difference and frictional pressure losses. Being complex mechanical components with moving parts, they are subject to wear and need more maintenance operations than other components; for this reason and their utmost importance for WDS operation, they usually have a degree of redundancy. A variety of valves is used for pressure regulation (pressure reducing valves and pressure safety valves), pipe isolation, flow direction control (check valves), flow rate control (flow control valves), and tank level control (altitude valves).

B. WDS Maintenance Procedures

Maintenance procedures are performed to restore normal operation after a contingency (relatively frequent in WDSs) or as a part of a preventive or evolutionary plan. Though the organization of procedures largely depends on the specific practice of each WDS operator, it can be effectively abstracted by an UML activity diagram composing activities along phases, with a low degree of concurrency, usually without cycles, and with durations bounded by contractual constraints.

For the purposes of this paper, we focus on pipe breakages, which are among the most critical failures in a WDS in terms of frequency, severity, and detectability [24]. In particular, we consider the five-phase maintenance procedure specified in Fig. 1, which reflects the guidelines issued by the U.S. Environmental Protection Agency [25] and the World Health Organization [26], [27]; in particular, the latter defines a repair procedure featuring pipe testing, cleaning, and disinfection, also providing appropriate timings for these operations.

1) The procedure starts with the phase of *Initial activities*: failure severity is evaluated based on the available information, e.g., a phone call notifying a water leakage. Needed manpower and tool resources are then gathered and sent on site; and, a pit/trench of sufficient depth is excavated to access and inspect the failed component.
2) The first physical intervention on the network comes in the *Topology modification* phase, where valves and pumps are managed to disconnect the failed pipe. On completion of these actions, each end user will be either *offline*, *online not served*, or *online served*, depending on whether it is disconnected from the WDS, connected but with pressure under contractual threshold, or connected and with sufficient pressure, respectively.
3) Repair actions are carried out during the *Pipe repair* phase: according to characteristics related to material, depth, and age, the failed pipe may be repaired by welding, or through external clamps, or it may be replaced; a sealing test is then performed and, if not passed, joints are checked and sealed again; next, the pipe is flushed to avoid contamination, with steps depending on the type of repair performed, with one possible repetition if the water quality test is not passed; after that, water is chlorinated, a test is performed to assess the chlorine concentration, and a short additional chlorination is repeated if the test is not passed; a final flush removes most of the chlorine and completes the repair phase.
4) During the *Topology restoration* phase, the pipe is reconnected to the water main.
5) The *Final activities* phase consists of backfilling the trench, paving, and completing administrative tasks to finalize the procedure.

For the value of generality, note that the procedure can be easily tailored to account for the repair of other components, such as valves and pumps, and all the steps of the proposed approach can be performed as well. In fact, in a single failure scenario, the repair of any failed component requires its isolation through a modification of the network topology, and the subsequent topology restoration as soon as repair is over. In

doing so, the procedure would be much similar to the UML activity diagram of Fig. 1, and would affect the WDS behavior only at topology changes, with no significant impact on the complexity of the subsequent stochastic model and analysis. Also note that the structure of the maintenance procedure is independent of the specific WDS topology and failed pipe, making stochastic analysis immune to the WDS complexity and finally permitting to address cases of real scale.

Execution times of repair activities largely depend on failed components, on topological and physical characteristics of the WDS, as well as on the practice of the specific utility companies involved. Data on the duration of maintenance operations are not easily found in the literature, mainly because they are not made explicit or kept undisclosed. Nevertheless, if an availability measure is to be estimated, at least the Mean Time To Repair (MTTR) is needed; to this end, various assumptions are made by researchers. Generally speaking, the correlation between diameter and MTTR proposed by [28] for iron cast pipes is widely used to estimate the mean value. In some cases, it is used as a deterministic value [29], [30]; whereas, where a probabilistic characterization is needed, uniform [31], exponential [32], or normal [33] distributions are assumed.

From a practical perspective, due to the increasing awareness of the value of empirical data on the execution times of maintenance activities, the practice of collecting such data on field is spreading. This is also supported by the growing availability of connected portable devices to be used in the work area. Moreover, some regulatory authorities are binding operators to collect data about broken pipes, response times, and repair times [34]. According to this, an increasing availability of more abundant and accurate data is to be expected.

Without loss of generality, we assume that durations with a large support can be specified as an expolynomial Probability Density Function (PDF) $f(x) = (x-a)(b-x)e^{-\lambda x}$, featuring a local maximum, a finite support $[a, b]$, and a null value at the borders, i.e., *Route traffic and excavate* ([1, 3] h), *Repair with clamps* ([2, 4] h), *Repair by welding* ([1, 3] h), *Replace pipe* ([2, 5] h), *Check and repair joints* ([1, 3] h), and *Backfill* ([1, 8] h). Conversely, for activities with a shorter support, a uniform distribution is used for the sake of simplicity, i.e., *Evaluate severity* ([1, 2] h), *Acquire resources* ([1, 2] h), *Disconnect pipe* ([0, 1] h), *Reconnect pipe* ([0, 1] h), and *Finalize procedure* ([0, 1] h). Finally, the duration of some activities can be safely approximated with a worst-case deterministic value, i.e., *Test sealing* (5 h), *Flush pipe* 1 (1 h or 10 h in case the pipe was repaired or replaced, respectively), *Test water quality* (0.5 h), *Flush pipe* 2 and *Flush pipe* 3 (2 h), *Chlorinate* (16 h), *Commission Test* (1 h), and *Short chlorinate* (6 h).

Each activity is also associated with a *daily time interval* specifying the times of day during which it can be executed, assuming that, when the interval is over, the activity is suspended to be resumed on the following day. Activities that are critical or do not require human intervention after manual activation are executed at any time (i.e., [0:00,24:00]), i.e., *Evaluate severity*, *Test sealing*, *Flush pipe*, *Chlorinate*, *Short chlorinate*, and *Reconnect pipe*. Other activities are performed during working hours (i.e., [8:00,18:00]), i.e., *acquire resources*, *Route traffic and excavate*, *Disconnect pipe*, and *Finalize procedure*. The remaining activities are executed during working and overtime hours (i.e., [8:00,22:00]) to reduce the outage time of end users. As a special case, *disconnect pipe* is the only activity that cannot be interrupted, since it is an atomic operation disconnecting the failed pipe from the WDS.

Alternative paths of the procedure are associated with probabilities, which we term *switch probabilities*. Specifically, in the selection of the pipe repair method based on the failure severity, *Repair with clamps*, *Repair by welding*, and *replace pipe* have probability 0.5, 0.45, and 0.05, respectively; in the evaluation of a test outcome (i.e., sealing test, water quality test, and chlorination test), the test is passed with probability 0.95 and failed with probability 0.05.

C. Separating the Stochastic and Hybrid Aspects

Operation and maintenance of a WDS involve both continuous and discrete dynamics: water flow in pipes and tank filling are governed by *deterministic* differential equations in *continuous* variables of pressure, velocity, and flow rate; however, during a maintenance, network topology, operation mode, and maintenance phases change at *discrete events*, with pumps switching on/off, valves changing state, working hours modifying the availability of personnel, maintenance procedures advancing through phases. The time points of many of these events are *stochastic* variables, e.g., the occurrence time of a contingency or the duration of a maintenance activity, hence the overall behavior falls in the class of SHSs [3]. In particular, in the specific problem addressed here: both the completions of the *Disconnect pipe* activity and the *Reconnect pipe* activity in the procedure of Fig. 1 occur at stochastic time points and affect network topology and performability measures of the overall system, thus comprising *spontaneous transitions* not affected by the continuous dynamics; water levels in tanks are the only continuous variables that hold memory of past history over a discrete transition, while all the other transitions *reset* the state to an absolute value statically determined either by the structure of the procedure or by the network topology and operation modes; and, pumps are switched on/off to start/stop tank filling when the tank level reaches a lower/upper threshold, thus comprising *forced transitions* triggered by the continuous dynamics.

To make solution feasible in the scale of a real application, the proposed approach separates stochastic and hybrid aspects: stochastic evaluation of the maintenance procedure determines the joint distribution of the time points when the network topology and operation mode are affected by spontaneous transitions; then, the distribution is fed to fluid-dynamic analysis, which encompasses continuous dynamics of physical quantities, memory induced by tanks levels, and forced transitions induced by control on thresholds on continuous quantities.

The Data Flow Diagram (DFD) shown in Fig. 2 illustrates the flow of information along the solution process.

1) The central transform is the *quantitative evaluation* of a dynamic-sTPN of the procedure, capturing the stochastic timing of repair activities (process 4, illustrated in

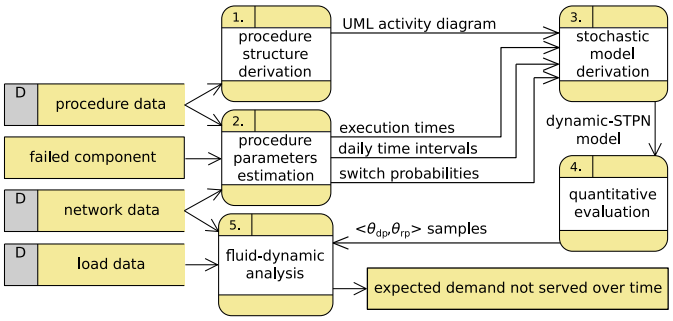

Fig. 2. DFD diagram of the solution method.

Sections III-C and III-D): specifically, simulation or analysis of the dynamic-sTPN evaluates the joint distribution of the completion times θ_{dp} and θ_{rp} of *Disconnect pipe* and *Reconnect pipe*, respectively, yielding paired samples $\langle \chi_{\text{dp}}, \chi_{\text{rp}} \rangle$ for the random vector $\langle \theta_{\text{dp}}, \theta_{\text{rp}} \rangle$, each associated with a measure of probability.

2) *Fluid-dynamic analysis* of the hybrid WDS behavior is then performed for each paired sample, based on the network topology and operation modes (*network data*) and on consumption profiles (*load data*) (process 5, discussed in Section IV-A); finally, the analysis results, quantifying the service lack experienced by users during the maintenance procedure, are weighted according to sample probabilities, enabling the evaluation of the expected DNS over time (Section IV-B).
3) In turn, the dynamic-sTPN model of the procedure is derived from the *UML activity diagram*, the *execution times*, the *daily time intervals*, and the *switch probabilities* (process 3, illustrated in Sections III-A and III-B): while the UML activity diagram is obtained only from *procedure data* (process 1, discussed in Section II-B), the procedure parameters are estimated using also *network data* and the identity of the *failed component* (process 2, also illustrated in Section II-B).

III. Evaluation of Stochastic Variables

In the procedure of Fig. 1, some activities may be suspended during nonworking hours and resumed the day after. This suspension could be naturally represented in a model based on the so-called Preemptive Resume (PR) policy [35] (also known as *enabling memory* or *age* policy [36]). Yet, in the specific application context, suspension is bound to have a deterministic duration and scheduled activities will eventually be completed. Modeling can thus be performed in a simpler way by extending the concept of *fickle functions* of [37] to a probabilistic setting. To this end, sTPNs [20] are augmented with fickle functions shifting the time-to-fire of persistent transitions by a deterministic value identified by the current marking and fired transition.

Moreover, sTPNs are also extended with: 1) *clocks* that can be reset by fired transitions, supporting the evaluation of the time elapsed between the completion of two activities, thus permitting the analytical derivation of the joint PDF of θ_{dp} and θ_{rp} and 2) *marking-dependent* Cumulative Distribution Functions (CDFs) used to sample the time-to-fire of newly enabled transitions, permitting to represent a different duration of the *Flush pipe 1* activity depending on whether the pipe was repaired or replaced. Following again the concepts of [37], the extended model is termed dynamic-sTPNs (presented in Section III-A). Note that both fickle functions and marking-dependent CDFs improve the modeling convenience without any substantial impact on the complexity of the method of stochastic state classes, while the presence of clocks requires an extension of this solution technique.

The dynamic-sTPN model of the maintenance procedure is derived through a disciplined approach (Section III-B) and analyzed through an extension of the method of stochastic state classes (Section III-C). The obtained state space permits to derive the symbolic form of the joint PDF of θ_{dp} and θ_{rp}, which is sampled over a regular grid (Section III-D).

A. Dynamic Stochastic Time Petri Nets

1) Syntax: A dynamic-sTPN is defined as a tuple $\langle P; T; A^{-}; A^{+}; A^{\cdot}; m_0; F; C; E; I, R, X, Y \rangle$, where:

1) P and T are the (disjoint) sets of places and transitions, respectively, while $A^{-} \subseteq P \times T$, $A^{+} \subseteq T \times P$, and $A^{\cdot} \subseteq P \times T$ are the sets of precondition, postcondition, and inhibitor arcs, respectively;
2) $m_0 : P \to \mathbb{N}$ is the initial marking assigning a number of tokens to each place;
3) $F : T \to [0,1]^{[\text{EFT}_{t,m}, \text{LFT}_{t,m}]^{\mathbb{N}^P}}$ associates each transition t with $F(t) : \mathbb{N}^P \to [0,1]^{[\text{EFT}_{t,m}, \text{LFT}_{t,m}]}$ which, in turn, associates each marking $m : P \to \mathbb{N}$ with a CDF $F_{t,m} : [\text{EFT}_{t,m}, \text{LFT}_{t,m}] \to [0,1]$, where $\text{EFT}_{t,m} \in \mathbb{Q}_0^+$ and $\text{LFT}_{t,m} \in \mathbb{Q}_0^+ \cup \{\infty\}$ are said *earliest* and a *latest firing time*, respectively;
4) $C : T \to \mathbb{R}^+$ associates each transition with a weight;
5) $E : T \to \{true, false\}^{\mathbb{N}^P}$ associates each transition t with an enabling function $E(t) : \mathbb{N}^P \to \{true, false\}$, in turn associating each marking with a Boolean value;
6) $I : T \to \mathbb{R}^{+\mathbb{N}^P \times T}$ associates each transition t with a *fickle function* $I(t) : (\mathbb{N}^P \times T) \to \mathbb{R}^+$ which, in turn, associates each marking and each (firing) transition with a nonnegative real valued additional delay;
7) $R : T \to \mathbb{N}$ associates each transition with a priority;
8) X is the set of clocks and $Y : T \to \mathcal{P}(X)$ associates each transition with a subset of clocks.

When the weight, the enabling function, the fickle function, the priority, or the subset of clocks are omitted for a transition t, we assume that $C(t) = 1$, $E(t)(m)$ evaluates to true for any marking m, $I(t)(m, t') = 0$ for any marking m and any transition $t' \neq t$, $R(t) = 0$, or $Y(t) = \emptyset$, respectively.

A place p is said an *input*, an *output*, or an *inhibitor* place for a transition t if $\langle p, t \rangle \in A^{-}$, $\langle t, p \rangle \in A^{+}$, or $\langle p, t \rangle \in A^{\cdot}$, respectively. A transition t newly enabled in a marking m is termed *immediate* (IMM) if $[\text{EFT}_{t,m}, \text{LFT}_{t,m}] = [0,0]$ and *timed* otherwise; if t is timed, it is said *exponential* (EXP) if $F_{t,m}(x) = 1 - e^{-\lambda x}$ over $[0, \infty]$ with $\lambda \in \mathbb{R}_0^+$ and *general* (GEN) otherwise; if t is GEN, it is termed *deterministic* (DET) if $\text{EFT}_{t,m} = \text{LFT}_{t,m}$ and *distributed* otherwise;

if t is distributed, we assume that $F_{t,m}$ is absolutely continuous over its support $[\mathrm{EFT}_{t,m}, \mathrm{LFT}_{t,m}]$, so that a PDF $f_{t,m}$ exists such that $F_{t,m}(x) = \int_0^x f_{t,m}(y)dy$.

2) Semantics: A transition is *enabled* by a marking if each of its input places contains at least one token, none of its inhibitor places contains any token, and its enabling function evaluates to true. The *state* of a dynamic-sTPN is a triplet $\langle m, \vec{\tau}, \vec{v}\rangle$, where: m is a marking; $\vec{\tau} \in \mathbb{R}_{\geq 0}^{|\mathcal{E}(m)|}$ associates each enabled transition with a time-to-fire, where $\mathcal{E}(m)$ is the set of transitions enabled by m; and, $\vec{v} \in \mathbb{R}_{\geq 0}^{|X|}$ associates each clock with a valuation. An enabled transitions t is *firable* in a state s if its time-to-fire is equal to zero and its priority is not lower than the priority of any other enabled IMM/DET transition with zero time-to-fire. When multiple transitions are firable, one of them is selected to fire with probability $\mathrm{Prob}\{t \text{ is selected}\} = \mathcal{C}(t)/\sum_{t_i \in \mathcal{F}(s)} \mathcal{C}(t_i)$, where $\mathcal{F}(s)$ is the set of firable transitions in s. When t fires, $s_1 = \langle m_1, \vec{\tau}_1, \vec{v}_1\rangle$ is replaced by $s_2 = \langle m_2, \vec{\tau}_2, \vec{v}_2\rangle$, where:

1) m_2 is derived from m_1 by removing a token from each input place of t, which yields an intermediate marking m_{tmp}, and by adding a token to each output place of t;
2) $\vec{\tau}_2$ is derived from $\vec{\tau}_1$ by: a) reducing the time-to-fire of each *persistent* transition t_p (i.e., enabled by m_{tmp} and m_2) by the time elapsed in s, and then adding the deterministic value $I(t_p)(m_2, t)$; b) sampling the time-to-fire of each *newly enabled* transition t_n (i.e., enabled by m_2 but not by m_{tmp}) according to its CDF F_{t_n,m_2} associated with marking m_2; and c) removing the time-to-fire of *disabled* transitions (i.e., not enabled by m_2);
3) $\vec{v}_2$ is derived from $\vec{v}_1$ by assigning zero to the valuation of each clock $x \in Y(t)$ and by adding the time elapsed in s to the valuation of each clock $x \notin Y(t)$.

B. Stochastic Model of the Repair Procedure

Fig. 3 shows the dynamic-sTPN model of the procedure specified by the UML activity diagram of Fig. 1 and the parameters defined in Section II-B. The *time of day submodel* represents the advancement of the hours of the day through a sequence of 24 DET transitions with firing time equal to 1, so that the firing of transition `Hour`N accounts for the stroke of the hour N:00, $\forall\ N \in \{0, 1, \ldots, 23\}$. In so doing, the start time of the procedure is specified by the initial marking, which assigns a token to place `hour`$((N+1)\%24)$ iff the procedure starts at N:00. Note that adjacent transitions could be merged as long as the submodel accounts for the procedure start time as well as the minimum start time and the maximum end time of any activity with daily time interval $\mathcal{I} \subset$[0:00,24:00].

The *activities submodel* accounts for sequencing and timing constraints of operations and it can be univocally derived from the *UML activity diagram*, the *execution times*, and the *daily time intervals* defined in Section II-B, thus being independent of the specific network topology and failed pipe. Specifically:

1) an activity a is represented by a transition t_a with the same PDF (e.g., transition `EvaluateSeverity` in Fig. 3 corresponds to the *Evaluate severity* activity in Fig. 1);
2) a sequence of activities is modeled by a sequence of transitions chained through their input places (e.g., transitions `EvaluateSeverity` and `AcquireResources` in Fig. 3);
3) a 1-to-n decision node is represented by a choice between n IMM transitions having a weight equal to the corresponding switch probability (e.g., transitions `CStart`, `WStart`, and `RStart` in Fig. 3 correspond to the repair strategy selection in Fig. 1 and have weight equal to 0.50, 0.45, and 0.05, respectively).

Moreover, for an activity a with daily time interval $\mathcal{I}_a = [i{:}00, j{:}00] \subset$ [0:00,24:00], with $i, j \in \mathbb{N}$ (e.g., the *Acquire resources* activity with daily time interval [8:00,18:00]):

1) the corresponding transition t_a has a fickle function that shifts its time-to-fire by $i + 24 - j$ upon the firing of transition `hour`j (belonging to the time of day submodel), in order to guarantee that a is suspended out of $\mathcal{I}_a$ (e.g., $\forall\ m \in \mathbb{N}^P$, $I(\texttt{AcquireResources})(m, t)$ equals 14 if $t =$ `Hour18`, and 0 otherwise);
2) an IMM transition t_a^{start} with an enabling function that evaluates to true if $\sum_{n=i+1}^{j} \mathtt{h}n == 1$ is chained with t_a, in order to guarantee that a is started within $\mathcal{I}_a$ (e.g., $\forall\ m \in \mathbb{N}^P$, $E(\texttt{ARStart})(m)$ equals *true* if $\sum_{n=9}^{18} m(\mathtt{h}n) == 1$ and *false* otherwise);
3) in the specific case that a cannot be suspended out of $\mathcal{I}_a$, t_a has no fickle function and t_a^{start} has an enabling function that evaluates to true if $\sum_{n=i+1}^{j-k} \mathtt{h}n == 1$, where k is the maximum execution time of a, in order to guarantee that a is started and completed within $\mathcal{I}_a$ (e.g., $\forall\ m \in \mathbb{N}^P$, $E(\texttt{DPStart})(m)$ is equal to *true* if $\sum_{n=9}^{17} m(\mathtt{h}n) == 1$ and *false* otherwise).

To avoid nondeterminism and reduce the state-space size, the DET transitions of the time of day submodel are associated with priority equal to 1, while those in the activities submodel are associated with the default priority 0.

It is worth noting that the dynamic-sTPN model of Fig. 3 is also added a clock c_{dp} that is reset upon the firing of transition `DisconnectPipe`, i.e., $Y(\texttt{DisconnectPipe}) = \{c_{\mathrm{dp}}\}$: in so doing, c_{dp} permits to represent the time elapsed from the completion time θ_{dp} of the *Disconnect pipe* activity to the completion time θ_{rp} of the *Reconnect pipe* activity, enabling the analytical evaluation of the joint PDF of θ_{dp} and θ_{rp}.

C. Stochastic State Classes With Clocks

The method of stochastic state classes [20], [21] samples the state of the marking process $\{M(t),\ t \geq 0\}$ of an sTPN after each transition firing ($M(t)$ is the marking at time t). Each sample is termed *stochastic state class* and encodes a marking plus a joint domain and a joint PDF for: 1) the vector $\vec{\tau}$ of the remaining times-to-fire of the enabled transitions and 2) a timer τ_{age}, accounting for the time elapsed since the entrance in the initial stochastic state class. Starting from an initial stochastic state class where $\tau_{\mathrm{age}} = 0$ and the times-to-fire of the enabled transitions are independently distributed according to expolynomial PDFs, a reachability relation is enumerated between stochastic state classes. According to the calculus of successor classes [38], in each stochastic state class, the random vector $\langle \vec{\tau}, \tau_{\mathrm{age}}\rangle$ turns out to be supported over a difference

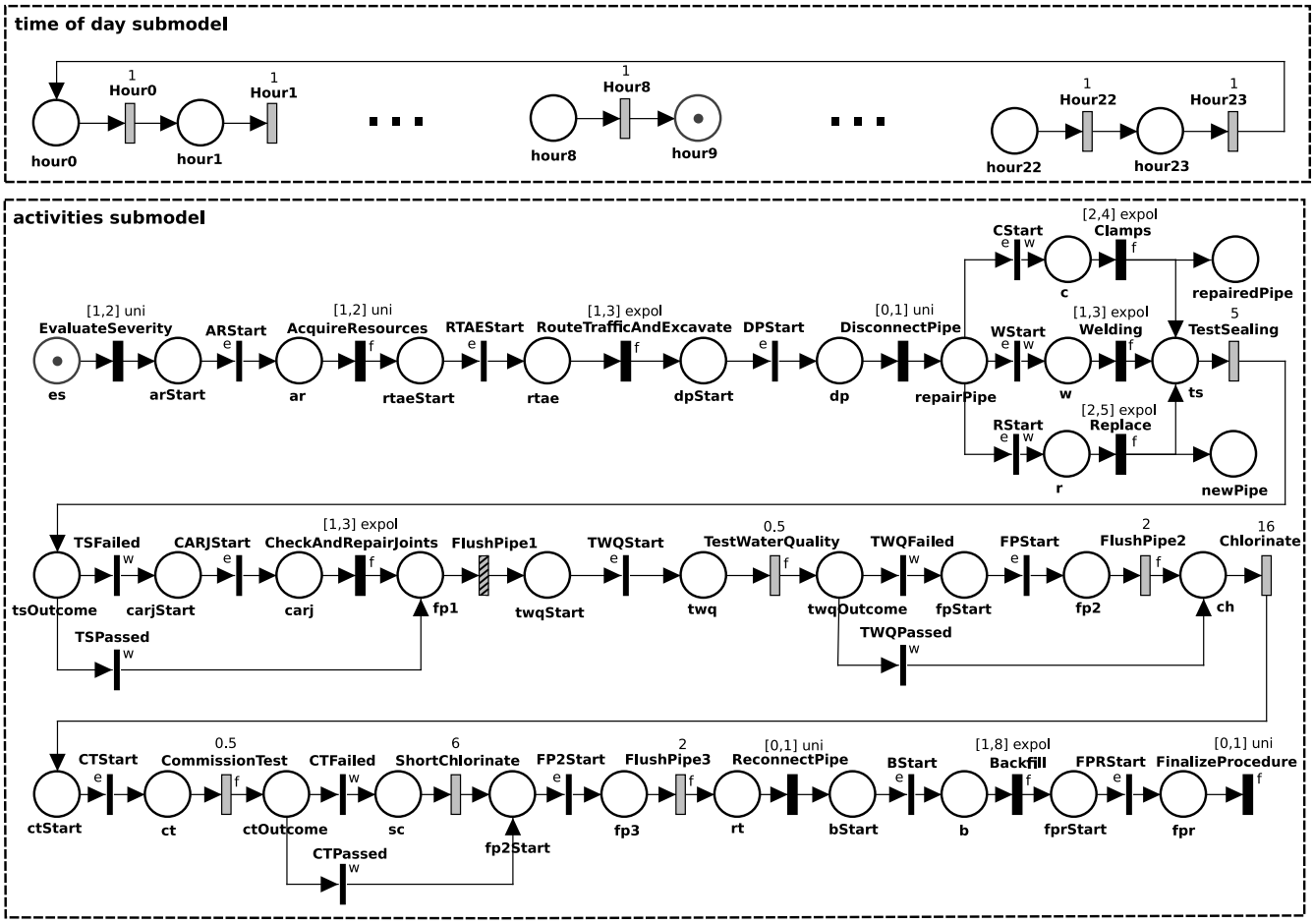

Fig. 3. Dynamic-sTPN model of the procedure specified by the UML activity diagram of Fig. 1 and the parameters defined in Section II-B, assuming that the start time is 8:00. IMM, DET, and GEN transitions are represented by thin black bars, thick gray bars, and thick black bars, respectively; in case the transition CDF is marking-dependent, the bar also has oblique stripes. Transitions associated with a not default value for enabling function, fickle function, and weight are marked with label "*e*," "*f*," and "*w*," respectively.

bounds matrix (DBM), i.e., a set of linear inequalities constraining the difference between pairs of timers, and distributed according to a PDF that accepts a piecewise representation over a partition of the support in DBM zones.

Fickle functions can be accounted in the solution technique by shifting the affected entries of the joint domain and PDF of $\langle \vec{\tau}, \tau_{\text{age}} \rangle$ by a deterministic value, which maintains the support of $\langle \vec{\tau}, \tau_{\text{age}} \rangle$ in a DBM form and its PDF in a piecewise representation over a partition of the support in DBM zones. Also marking-dependent CDFs can be accounted in a straightforward manner, by associating the time-to-fire of newly enabled transitions with a different PDF depending on the current marking. Conversely, the presence of clocks augments the random vector $\langle \vec{\tau}, \tau_{\text{age}} \rangle$ with clock valuations $\vec{v}$, requiring to extend the concept of stochastic state class, the reachability relation between stochastic state classes, and the calculus of the successors of a stochastic state class.

Definition 1: A *stochastic state class* (class for short) is a triplet $\Sigma = \langle m, D_{\langle \vec{\tau}, \tau_{\text{age}}, \vec{v} \rangle}, f_{\langle \vec{\tau}, \tau_{\text{age}}, \vec{v} \rangle} \rangle$ where: $m \in \mathbb{N}^P$ is a marking; $D_{\langle \vec{\tau}, \tau_{\text{age}}, \vec{v} \rangle} \subseteq (\mathbb{R}_{\geq 0})^{|\mathcal{E}(m)|} \times (\mathbb{R}_{\leq 0})^{1+|X|}$ is the support of the random vector $\langle \vec{\tau}, \tau_{\text{age}}, \vec{v} \rangle$ made of the remaining times-to-fire $\vec{\tau}$ of the transitions enabled by m, τ_{age}, and the clock valuations $\vec{v}$; $f_{\langle \vec{\tau}, \tau_{\text{age}}, \vec{v} \rangle}$ is the PDF of $\langle \vec{\tau}, \tau_{\text{age}}, \vec{v} \rangle$.

Definition 2: $\Sigma' = \langle m', D'_{\langle \vec{\tau}', \tau'_{\text{age}}, \vec{v}' \rangle}, f'_{\langle \vec{\tau}', \tau'_{\text{age}}, \vec{v}' \rangle} \rangle$ is the successor of $\Sigma = \langle m, D_{\langle \vec{\tau}, \tau_{\text{age}}, \vec{v} \rangle}, f_{\langle \vec{\tau}, \tau_{\text{age}}, \vec{v} \rangle} \rangle$ through transition t_1 with probability μ_1, i.e., $\Sigma \overset{t_1, \mu_1}{\Rightarrow} \Sigma'$, iff the following property holds: if the marking of the dynamic-sTPN is m and the random vector $\langle \vec{\tau}, \tau_{\text{age}}, \vec{v} \rangle$ is distributed over $D_{\langle \vec{\tau}, \tau_{\text{age}}, \vec{v} \rangle}$ according to $f_{\langle \vec{\tau}, \tau_{\text{age}}, \vec{v} \rangle}$, the firing of t_1 occurs with probability μ_1 in Σ, yielding marking m' and a random vector $\langle \vec{\tau}', \tau'_{\text{age}}, \vec{v}' \rangle$ distributed over $D'_{\langle \vec{\tau}', \tau'_{\text{age}}, \vec{v}' \rangle}$ according to $f'_{\langle \vec{\tau}', \tau'_{\text{age}}, \vec{v}' \rangle}$.

Given a succession relation $\Sigma \overset{t_1, \mu_1}{\Rightarrow} \Sigma'$, class Σ' is derived from class Σ by extending the calculus of successor classes [20] according to the dynamic-sTPN semantics of Section III-A. The computation consists of four steps.

1) Condition the random vector $\langle \vec{\tau}, \tau_{\text{age}}, \vec{v} \rangle$ to the assumption that t_1 is the next transition to fire, yielding a new random vector $\langle \vec{\tau}^a, \tau^a_{\text{age}}, \vec{v}^a \rangle$ (*conditioning*).
2) Reduce the $\langle \vec{\tau}^a, \tau^a_{\text{age}}, \vec{v}^a \rangle$ entries by the time elapsed in Σ (i.e., the time-to-fire of t_1) and eliminate the time-to-fire of the fired transition t_1, yielding $\langle \vec{\tau}^b, \tau^b_{\text{age}}, \vec{v}^b \rangle$, and then increment some of the $\langle \vec{\tau}^b, \tau^b_{\text{age}}, \vec{v}^b \rangle$ entries by a deterministic value according to the fickle functions, yielding $\langle \vec{\tau}^c, \tau^c_{\text{age}}, \vec{v}^c \rangle$ (*time advancement and projection*).

3) Eliminate the times-to-fire of the disabled transitions from $\langle \vec{\tau}^c, \tau^c_{\text{age}}, \vec{v}^c \rangle$, yielding $\langle \vec{\tau}^d, \tau^d_{\text{age}}, \vec{v}^d \rangle$ (*disabling*).
4) Augment $\langle \vec{\tau}^d, \tau^d_{\text{age}}, \vec{v}^d \rangle$ with the times-to-fire of the newly enabled transitions, finally yielding the random vector $\langle \vec{\tau}', \tau'_{\text{age}}, \vec{v}' \rangle$ (*newly enabling*).

For readability, technical details on the steps of derivation of successor classes are reported in the Appendix.

The succession relation $\overset{t,\mu}{\Longrightarrow}$ is enumerated from the initial class $\Sigma_0 = \langle m_0, D^0_{\langle \vec{\tau}, \tau_{\text{age}}, \vec{v} \rangle}, f^0_{\langle \vec{\tau}, \tau_{\text{age}}, \vec{v} \rangle} \rangle$, where $\vec{\tau}$, τ_{age}, and $\vec{v}$ are independently distributed, yielding a *transient tree* where each enumerated class $\Sigma = \langle m, D_{\langle \vec{\tau}, \tau_{\text{age}}, \vec{v} \rangle}, f_{\langle \vec{\tau}, \tau_{\text{age}}, \vec{v} \rangle} \rangle$ represents a node, with the elements of the random vector $\langle \vec{\tau}, \tau_{\text{age}}, \vec{v} \rangle$ being mutually dependent random variables, and each succession relation $\Sigma \overset{t,\mu}{\Rightarrow} \Sigma'$ represents an edge from node Σ to node Σ', labeled with the fired transition t and the corresponding firing probability μ. The calculus of successor classes according to the dynamic-sTPN semantics performs on the random vector $\langle \vec{\tau}, \tau_{\text{age}}, \vec{v} \rangle$ the same types of operation performed on the random vector $\langle \vec{\tau}, \tau_{\text{age}} \rangle$ by the calculus according to the sTPN semantics (e.g., reducing each time-to-fire by the time-to-fire of the fired transition, eliminating a time-to-fire through a projection, adding a time-to-fire distributed independently of the already present times-to-fire). Therefore, in each enumerated class $\Sigma = \langle m, D_{\langle \vec{\tau}, \tau_{\text{age}}, \vec{v} \rangle}, f_{\langle \vec{\tau}, \tau_{\text{age}}, \vec{v} \rangle} \rangle$, $D_{\langle \vec{\tau}, \tau_{\text{age}}, \vec{v} \rangle}$ is a DBM and $f_{\langle \vec{\tau}, \tau_{\text{age}}, \vec{v} \rangle}$ takes a continuous piecewise representation over a partition of $D_{\langle \vec{\tau}, \tau_{\text{age}}, \vec{v} \rangle}$ in DBM zones. The *reaching probability* of a class Σ_n reached from the initial class Σ_0 through the sequence of firings $\Sigma_0 \overset{t_1,\mu_1}{\Longrightarrow} \Sigma_1 \overset{t_2,\mu_2}{\Longrightarrow} \dots \overset{t_n,\mu_n}{\Longrightarrow} \Sigma_n$ is $\eta_n = \prod_{i=1}^{n} \mu_i$.

D. Sampling of the Joint PDF of Stochastic Variables

Evaluation of the distribution of the time intervals during which the WDS topology and behavior are affected by the procedure requires the identification of the joint support $D_{\langle \theta_{\text{dp}}, \theta_{\text{rp}} \rangle}$ and the joint PDF $f_{\langle \theta_{\text{dp}}, \theta_{\text{rp}} \rangle}$ of the time points at which the *Disconnect pipe* and the *Reconnect pipe* activities are completed. These can be derived from the transient tree of the dynamic-sTPN model of the procedure, and specifically from the set $\mathcal{I}$ of stochastic state classes reached through any firing sequence terminated by the transition `ReconnectPipe`. By construction, in each class $\Sigma_i = \langle m^i, D^i_{\langle \vec{\tau}, \tau_{\text{age}}, v_{\text{dp}} \rangle}, f^i_{\langle \vec{\tau}, \tau_{\text{age}}, v_{\text{dp}} \rangle} \rangle \in \mathcal{I}$, the following relations subsist among timers.[1]

1) The value of τ_{age} represents the opposite of the time elapsed from the beginning of the procedure until the completion of *Reconnect pipe*; therefore, the completion time of *Reconnect pipe* can be evaluated as $\theta_{\text{rp}} = -\tau_{\text{age}}$.
2) The value v_{dp} of clock c_{dp} (defined at the end of Section III-B) represents the opposite of the time elapsed from the completion of *Disconnect pipe* until the completion of *Reconnect pipe*; therefore, the completion time of *Disconnect pipe* can be evaluated as $\theta_{\text{dp}} = -\tau_{\text{age}} + v_{\text{dp}}$.

[1] According to the calculus of successor classes developed in the Appendix, in each class $\Sigma = \langle m, D_{\langle \vec{\tau}, \tau_{\text{age}}, \vec{v} \rangle}, f_{\langle \vec{\tau}, \tau_{\text{age}}, \vec{v} \rangle} \rangle$, τ_{age} and $\vec{v}$ encode the opposite of the elapsed time and the opposite of the clock values, respectively.

According to this, the joint domain $D^i_{\langle \theta_{\text{dp}}, \theta_{\text{rp}} \rangle}$ and the joint PDF $f^i_{\langle \theta_{\text{dp}}, \theta_{\text{rp}} \rangle}$ of θ_{dp} and θ_{rp} in each class $\Sigma_i \in \mathcal{I}$ can be derived through a projection and a linear transformation from $D^i_{\langle \vec{\tau}, \tau_{\text{age}}, v_{\text{dp}} \rangle}$ and $f^i_{\langle \vec{\tau}, \tau_{\text{age}}, v_{\text{dp}} \rangle}$, respectively

$$D^i_{\langle \theta_{\text{dp}}, \theta_{\text{rp}} \rangle}(z_{\text{dp}}, z_{\text{rp}}) = \bar{D}^i_{\langle \tau_{\text{age}}, v_{\text{dp}} \rangle}\left(-x_{\text{age}} + y_{\text{dp}}, -x_{\text{age}}\right) \quad (1)$$

$$f^i_{\langle \theta_{\text{dp}}, \theta_{\text{rp}} \rangle}(z_{\text{dp}}, z_{\text{rp}}) = \bar{f}^i_{\langle \tau_{\text{age}}, v_{\text{dp}} \rangle}\left(-x_{\text{age}} + y_{\text{dp}}, -x_{\text{age}}\right) \quad (2)$$

where $\bar{D}^i_{\langle \tau_{\text{age}}, v_{\text{dp}} \rangle}$ is the projection of $D^i_{\langle \vec{\tau}, \tau_{\text{age}}, v_{\text{dp}} \rangle}$ that eliminates the variables in $\vec{\tau}$ (i.e., the times-to-fire of the transitions enabled by marking m^i) from the random vector $\langle \vec{\tau}, \tau_{\text{age}}, v_{\text{dp}} \rangle$, and $\bar{f}^i_{\langle \tau_{\text{age}}, v_{\text{dp}} \rangle}(x_{\text{age}}, y_{\text{dp}}) = \int_{D^i_{\langle \vec{\tau}, \tau_{\text{age}}, v_{\text{dp}} \rangle}} f^i_{\langle \vec{\tau}, \tau_{\text{age}}, v_{\text{dp}} \rangle}(\vec{x}, x_{\text{age}}, y_{\text{dp}})\, d\vec{x}$ is the marginal PDF of $\langle \tau_{\text{age}}, v_{\text{dp}} \rangle$. Given that $D^i_{\langle \vec{\tau}, \tau_{\text{age}}, v_{\text{dp}} \rangle}$ is a DBM domain and $f^i_{\langle \vec{\tau}, \tau_{\text{age}}, v_{\text{dp}} \rangle}$ accepts a piecewise representation over a partition of $D^i_{\langle \vec{\tau}, \tau_{\text{age}}, v_{\text{dp}} \rangle}$ in DBM zones, also $D^i_{\langle \theta_{\text{dp}}, \theta_{\text{rp}} \rangle}$ is DBM shaped and $f^i_{\langle \theta_{\text{dp}}, \theta_{\text{rp}} \rangle}$ has a piecewise representation over a partition of $D^i_{\langle \theta_{\text{dp}}, \theta_{\text{rp}} \rangle}$ in DBM zones. Finally, $D_{\langle \theta_{\text{dp}}, \theta_{\text{rp}} \rangle}$ is obtained as the union of domains $D^i_{\langle \theta_{\text{dp}}, \theta_{\text{rp}} \rangle}$ of classes $\Sigma_i \in \mathcal{I}$, and $f_{\langle \theta_{\text{dp}}, \theta_{\text{rp}} \rangle}$ is computed as the sum of the corresponding PDFs $f^i_{\langle \theta_{\text{dp}}, \theta_{\text{rp}} \rangle}$, each weighted by the reaching probability η_i of Σ_i

$$D_{\langle \theta_{\text{dp}}, \theta_{\text{rp}} \rangle} = \bigcup_{i \in \mathcal{I}} D^i_{\langle \theta_{\text{dp}}, \theta_{\text{rp}} \rangle} \quad (3)$$

$$f_{\langle \theta_{\text{dp}}, \theta_{\text{rp}} \rangle}(z_{\text{dp}}, z_{\text{rp}}) = \sum_{i \in \mathcal{I}} \eta_i f^i_{\langle \theta_{\text{dp}}, \theta_{\text{rp}} \rangle}(z_{\text{dp}}, z_{\text{rp}}). \quad (4)$$

By construction, $\int_{D_{\langle \theta_{\text{dp}}, \theta_{\text{rp}} \rangle}} f_{\langle \theta_{\text{dp}}, \theta_{\text{rp}} \rangle}(z_{\text{dp}}, z_{\text{rp}})\, dz_{\text{dp}}\, dz_{\text{rp}} = 1$.

The transient tree of the dynamic-sTPN model of Fig. 3 is enumerated through the ORIS Tool [39] (30 s using a single core of a 2.67 GHz Intel Xeon E5640 processor), yielding 222 classes, overall partitioned into 898 DBM zones. Fig. 4 plots in gray the support $D_{\langle \theta_{\text{dp}}, \theta_{\text{rp}} \rangle}$, computed from the transient tree according to (3) and (4). On the one hand, θ_{dp} takes values between 3 h and 8 h, as it could be deduced also from the model, given that `DisconnectPipe` has an execution time interval equal to $[0, 1]$ h and it is preceded by three activities that have an overall execution time interval equal to $[3, 7]$ h and, according to their work schedules, are never suspended when the procedure starts at 8:00. On the other hand, θ_{rp} has a much wider interval comprised between 29 and 81.5 h, not only due to the greater number of activities that precede `ReconnectPipe`, but also as an effect of the conditional execution of some activities and the suspension during the night. Note that night stops of repair activities cut entire slices from $D_{\langle \theta_{\text{dp}}, \theta_{\text{rp}} \rangle}$, so that it is not a connected space: for instance, if the failed pipe is disconnected from the WDS 4 h after the procedure start (i.e., $\theta_{\text{dp}} = 4$ h), it may be the case that it is reconnected after 33 h (i.e., $\theta_{\text{rp}} = 37$ h) or after 51 h (i.e., $\theta_{\text{rp}} = 55$ h), but not after 61 h (i.e., $\theta_{\text{rp}} = 65$ h).

The joint PDF $f_{\langle \theta_{\text{dp}}, \theta_{\text{rp}} \rangle}$ of θ_{dp} and θ_{rp} is sampled according to a regular grid Γ, defined over the minimum DBM that embeds $D_{\langle \theta_{\text{dp}}, \theta_{\text{rp}} \rangle}$ and made of equispaced points with step $\delta\theta_{\text{dp}}$ and $\delta\theta_{\text{rp}}$ for θ_{dp} and θ_{rp}, respectively (in Fig. 4(b), $\delta\theta_{\text{dp}} = 1$ h and $\delta\theta_{\text{rp}} = 5$ h). Each point $\langle \chi_{\text{dp}}, \chi_{\text{rp}} \rangle \in \Gamma$ is associated with a measure of probability $\gamma_{\langle \chi_{\text{dp}}, \chi_{\text{rp}} \rangle}$.

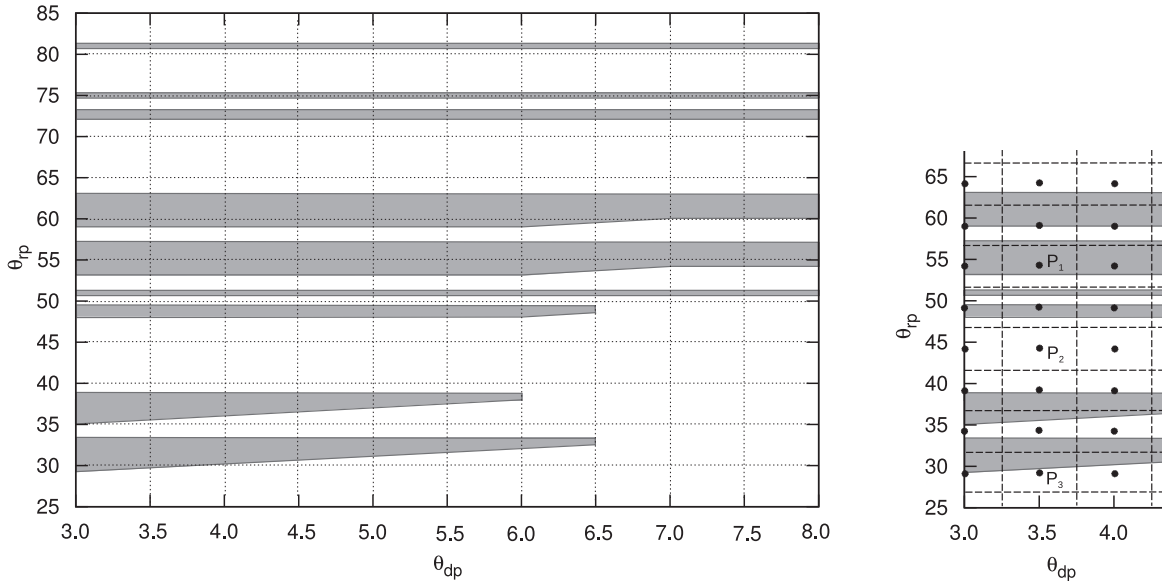

Fig. 4. (a) Joint domain of the stochastic times when the maintenance procedure specified by the dynamic-sTPN model of Fig. 3 affects the WDS behavior (times expressed in h), i.e., the joint domain $D_{\langle\theta_{\rm dp},\theta_{\rm rp}\rangle}$ of the completion times $\theta_{\rm dp}$ and $\theta_{\rm rp}$ of *Disconnect pipe* and *Reconnect pipe* in the UML activity diagram of Fig. 1, respectively, represented by the firing of transitions `DisconnectPipe` and `ReconnectPipe` in Fig. 3, respectively. (b) Fragment of the domain of Fig. 4(a) and a regular grid Γ of equally spaced points with step $\delta\theta_{\rm dp} = 1\,{\rm h}$ and $\delta\theta_{\rm rp} = 5\,{\rm h}$ for $\theta_{\rm dp}$ and $\theta_{\rm rp}$, respectively.

1) If $\langle\chi_{\rm dp}, \chi_{\rm rp}\rangle \in D_{\langle\theta_{\rm dp},\theta_{\rm rp}\rangle}$ (e.g., $P_1 = \langle 3.5\,{\rm h}, 54\,{\rm h}\rangle$ in Fig. 4(b)), then $\langle\chi_{\rm dp}, \chi_{\rm rp}\rangle$ is associated with the integral of $f_{\langle\theta_{\rm dp},\theta_{\rm rp}\rangle}$ over the intersection between $D_{\langle\theta_{\rm dp},\theta_{\rm rp}\rangle}$ and the $\delta\theta_{\rm dp} \times \delta\theta_{\rm rp}$ rectangle $\mathcal{R}_{\langle\chi_{\rm dp},\chi_{\rm rp}\rangle}$ centered in $\langle\chi_{\rm dp}, \chi_{\rm rp}\rangle$

$$\gamma_{\langle\chi_{\rm dp},\chi_{\rm rp}\rangle} = \int_{\mathcal{R}_{\langle\chi_{\rm dp},\chi_{\rm rp}\rangle}\cap D_{\langle\theta_{\rm dp},\theta_{\rm rp}\rangle}} f_{\langle\theta_{\rm dp},\theta_{\rm rp}\rangle}(z_{\rm dp}, z_{\rm rp})\, dz_{\rm dp}\, z_{\rm rp} \quad (5)$$

where $\mathcal{R}_{\langle\chi_{\rm dp},\chi_{\rm rp}\rangle} = \{\langle z_{\rm dp}, z_{\rm rp}\rangle \in \mathbb{R}^2 \,|\, \chi_{\rm dp} - \delta\theta_{\rm dp}/2 \le z_{\rm dp} \le \chi_{\rm dp} + \delta\theta_{\rm dp}/2,\ \chi_{\rm rp} - \delta\theta_{\rm rp}/2 \le z_{\rm rp} \le \chi_{\rm rp} + \delta\theta_{\rm rp}/2\}$.

2) If $\langle\chi_{\rm dp}, \chi_{\rm rp}\rangle \notin D_{\langle\theta_{\rm dp},\theta_{\rm rp}\rangle}$ and $\mathcal{R}_{\langle\chi_{\rm dp},\chi_{\rm rp}\rangle} \cap D_{\langle\theta_{\rm dp},\theta_{\rm rp}\rangle} = \emptyset$ (e.g., $P_2 = \langle 3.5\,{\rm h}, 44\,{\rm h}\rangle$ in Fig. 4(b)), then $\langle\chi_{\rm dp}, \chi_{\rm rp}\rangle$ is associated with a null probability, i.e., $\gamma_{\langle\chi_{\rm dp},\chi_{\rm rp}\rangle} = 0$.

3) If $\langle\chi_{\rm dp}, \chi_{\rm rp}\rangle \notin D_{\langle\theta_{\rm dp},\theta_{\rm rp}\rangle}$ and $\mathcal{R}_{\langle\chi_{\rm dp},\chi_{\rm rp}\rangle} \cap D_{\langle\theta_{\rm dp},\theta_{\rm rp}\rangle} \neq \emptyset$ (e.g., $P_3 = \langle 3.5\,{\rm h}, 29\,{\rm h}\rangle$ in Fig. 4(b)), the integral $\gamma_{\langle\chi_{\rm dp},\chi_{\rm rp}\rangle}$ of $f_{\langle\theta_{\rm dp},\theta_{\rm rp}\rangle}$ over $\mathcal{R}_{\langle\chi_{\rm dp},\chi_{\rm rp}\rangle} \cap D_{\langle\theta_{\rm dp},\theta_{\rm rp}\rangle}$, defined in (5), is associated with the point $\langle\chi_{\rm dp}, \tilde{\chi}_{\rm rp}\rangle$ such that $\langle\chi_{\rm dp}, \tilde{\chi}_{\rm rp}\rangle \in D_{\langle\theta_{\rm dp},\theta_{\rm rp}\rangle}$ and $|\chi_{\rm rp} - \tilde{\chi}_{\rm rp}|$ is minimum. Note that, for the purposes of the subsequent treatment, the new point is intentionally selected by leaving the value of $\theta_{\rm dp}$ unchanged, so that the set of possible values of $\theta_{\rm dp}$ for the points of the grid is known *a priori* (i.e., before the grid is constructed). Also note that, as shown in Fig. 4, such a point $\langle\chi_{\rm dp}, \tilde{\chi}_{\rm rp}\rangle$ always exists: in fact, given a value $\chi_{\rm dp} \in [3, 8]\,{\rm h}$ for $\theta_{\rm dp}$, it is never the case that $\{\langle z_{\rm dp}, z_{\rm rp}\rangle \in \mathbb{R}^2 | z_{\rm dp} = \chi_{\rm dp}\} \cap D_{\langle\theta_{\rm dp},\theta_{\rm rp}\rangle} = \emptyset$.

IV. Performability Evaluation

A. Fluid-Dynamic Model and Analysis

From a modeling point of view, the piping of a WDS is envisaged as a graph where pipes, pumps, and valves are represented as edges, whereas junctions between pipes, load nodes, tanks, and reservoirs are represented as nodes. At any given instant, the network state is defined by its topology (active and closed edges), water pressure at all nodes, flow rate in all edges, tank levels, and pump states (on/off). While tank levels are system state variables that depend on its history, water pressures and flow rates are calculated based on the network characteristics and the boundary conditions represented by nodal demands and pump states. To calculate pressure at all nodes and flow rate in all edges, three sets of equations are defined [1], considering International System (SI) units in each of them. In particular, lengths, diameters, and pressures (hydraulic heads) are expressed in meters (m) while mass flow rates and nodal demands in cubic meters per second (m^3/s). Most equations hold also if another consistent measurement system is used; when this is not the case an explicit warning will be given.

1) Mass Conservation at Memoryless Nodes: For each node, the algebraic sum of entering and exiting flow rates must equal zero or the nodal demand, depending on whether the node is a junction or represents a user, respectively, i.e., for node k, the following equation holds:

$$\sum_{i\in I_k} Q_{ik}(t) - \sum_{j\in O_k} Q_{kj}(t) = \begin{cases} 0 & \text{if junction} \\ Q_k^{\rm D}(t) & \text{if load node} \end{cases} \quad (6)$$

where I_k is the set of indexes of edges entering node k, O_k is the set of indexes of edges leaving the node, $Q_{ik}(t)$ is the flow rate from node i to node k at time t, and $Q_k^{\rm D}(t)$ is the nodal demand of node k at time t.

2) Pressure Loss/Gain Along Edges: For each edge, an equation relating the flow rate along the edge and the pressure difference at the start and the end nodes is needed. For pipes, the Hazen-Williams equation is considered, which is commonly used in the industrial practice for water flowing in cylindric pipes, i.e., for edge k leaving node i and entering

node j, the following equation holds:

$$H_i(t) - H_j(t) = \text{sign}[Q_{ij}(t)] \frac{10.67\, L_k}{{C_k}^{1.852} {d_k}^{4.871}} |Q_{ij}(t)|^{1.85} \tag{7}$$

where $H_i(t)$ is the pressure at node i at time t, L_k is the pipe length, d_k is the pipe inner diameter, and C_k is the Hazen-Williams coefficient for the pipe, which depends on the pipe material and the surface roughness. The coefficient 10.67 is valid for SI units; if other systems of units are used, the corresponding coefficient can be found in the literature or can be calculated.

For pumps, a specific correlation relating the pumped flow rate and the pressure difference is needed, usually obtained by interpolation of experimental data, i.e., for pump k, the following equation holds:

$$Q_{ij}(t) = \begin{cases} f_k\big(H_i(t) - H_j(t)\big) & \text{if pump is on} \\ 0 & \text{if pump is off} \end{cases} \tag{8}$$

where $f_k(x)$ is a function referring to the specific pump k and experimentally determined by the manufacturer.

3) Tank Characteristic Equation: Tanks are the elements of the system that hold memory of past history, with pressure at the corresponding nodes changing in time due to incoming or exiting flow rates. Each tank k is characterized by a function S_k depending on its cross section which, in turn, varies with the height, so that

$$\frac{\mathrm{d}H_k}{\mathrm{d}t} = \frac{\sum_{I_k} Q_{ik}(t) - \sum_{O_k} Q_{kj}(t)}{S_k(H_k(t))} \tag{9}$$

where $S_k(H)$ is the tank cross section corresponding to a water head H. Note that hydraulic heads (dimensionally corresponding to heights), tank cross sections (areas), and volumes must be expressed by appropriate powers of the same unit length, e.g., meters or feet.

Due to the complexity of the problem, formulated by nonlinear algebraic and differential equations, its solution is derived by dividing the analysis timespan into steps. To this end, the WDS is considered to be in steady-state within each time step, introducing an approximation error that can be neglected as long as the time step is short compared with the characteristic time constants of the WDS. By the steady-state hypothesis within a time step, the system is therefore solved iteratively with the right terms of the last set of equations equal to zero, yielding pressures and flow rates. Tank levels and pump states are then updated according to the solution, and the system is solved for the following time step.

Fluid-dynamic analysis of WDSs is supported by a number of commercial tools, e.g., WaterCAD [40] and KyPipes [41], and by some free tool, e.g., Transparent Blue WatDis [42] and EPANET [43]. In this paper, we have used EPANET, a widespread tool both in the academy and in industry, released by the U.S. Environmental Protection Agency. EPANET supports the solution of the system of differential equations, determining pressures, flow rates, tank levels, switch states etc. once the WDS topology and the boundary conditions (water demand) are known. The system is solved iteratively using a sparse matrix method derived from the Newton-Raphson method, based on node reordering with analytical calculation of the Jacobian matrix. Specifically, the WDS behavior is analyzed as a function of time, adjusting the analysis time step to take into account state changes of the active components. The output consists of a set of nodal pressures and pipe flow rates for each report time step. To achieve a proper understanding of the network behavior, the report time step must be much shorter than the system time constants, which mainly depend on tank sizes.

B. Measure Definition and Evaluation

While the quality of service delivered to end users is typically evaluated by focusing on the perspective of the single customer [44] (e.g., estimating the average interruption rate or duration), the global impact of a maintenance procedure in the transient phase following a failure is inherently assessed through a system-wide measure of the perceived performance. Users perceive defective service when water is required but not supplied, or when it is supplied with an insufficient pressure and they are not equipped with a local pumping device. Hence, we define the DNS at time t as

$$\text{DNS}(t) = \sum_{i|H_i(t)<H_{\min}} Q_i^{\text{D}}(t) \cdot \min\left\{ \frac{H_{\min} - H_i(t)}{H_{\min} - H_{\text{th}}}, 1 \right\} \tag{10}$$

where: $H_i(t)$ is the pressure at node i at time t, derived through fluid-dynamic analysis as illustrated in Section IV-A; $H_{\min}$ is the minimum contractual pressure; $H_{\text{th}} < H_{\min}$ is a pressure threshold below which a node is considered fully not-served; and, $Q_i^{\text{D}}(t)$ is the water demand of node i at time t, which is a constant value known from boundary conditions. According to this, DNS(t) is a weighted summation of the water demand of the nodes that are not adequately served, where the weight is a linear coefficient varying from 0, for nodes featuring the required pressure level H_{req}, to 1, for nodes with pressure not greater than H_{th}, for which the DNS is computed entirely. Therefore, DNS(t) is also expressed in flow rate units (m^3/s in SI).

For each time t, we evaluate the expected value of DNS(t), which we denote as $\Omega(t)$

$$\Omega(t) \stackrel{\text{def}}{=} \text{E}[\text{DNS}(t)] = \int_{z=0}^{\infty} z f_{\text{DNS}(t)}(z)\, dz \tag{11}$$

where $f_{\text{DNS}(t)}$ is the PDF of DNS(t). Again, the expected value of DNS(t) is expressed in flow rate units (m^3/s in SI). By the theorem of total probability, (11) can be rewritten as

$$\Omega(t) = \int_{z=0}^{\infty} z \int_{z_{\text{dp}}=0}^{\infty} \int_{z_{\text{rp}}=0}^{\infty} f_{\text{DNS}(t)|\langle z_{\text{dp}}, z_{\text{rp}}\rangle}(z) \cdot f_{\langle \theta_{\text{dp}}, \theta_{\text{rp}}\rangle}(z_{\text{dp}}, z_{\text{rp}})\, dz_{\text{rp}}\, dz_{\text{dp}}\, dz. \tag{12}$$

Note that $\text{DNS}(t) \mid \langle z_{\text{dp}}, z_{\text{rp}}\rangle$ is a determined value, with time t supported over the time span of interest for the analysis and $\langle z_{\text{dp}}, z_{\text{rp}}\rangle$ supported over $D_{\langle \theta_{\text{dp}}, \theta_{\text{rp}}\rangle}$. Specifically, it can be computed according to (10) through a run of EPANET

for all time values of interest. According to this, its PDF is $f_{\mathrm{DNS}(t)|\langle z_{\mathrm{dp}}, z_{\mathrm{rp}}\rangle}(z) = \delta(z - \mathrm{DNS}(t) \mid \langle z_{\mathrm{dp}}, z_{\mathrm{rp}}\rangle)$, yielding

$$\Omega(t) = \int_{z_{\mathrm{dp}}=0}^{\infty} \int_{z_{\mathrm{rp}}=0}^{\infty} f_{\langle \theta_{\mathrm{dp}}, \theta_{\mathrm{rp}}\rangle}(z_{\mathrm{dp}}, z_{\mathrm{rp}}) \cdot \int_{z=0}^{\infty} z f_{\mathrm{DNS}(t)|\langle z_{\mathrm{dp}}, z_{\mathrm{rp}}\rangle}(z)\, dz \;\; dz_{\mathrm{rp}}\, dz_{\mathrm{dp}}. \tag{13}$$

By the properties of the Dirac delta function, we finally obtain

$$\Omega(t) = \int_{z_{\mathrm{dp}}=0}^{\infty} \int_{z_{\mathrm{rp}}=0}^{\infty} f_{\langle \theta_{\mathrm{dp}}, \theta_{\mathrm{rp}}\rangle}(z_{\mathrm{dp}}, z_{\mathrm{rp}}) \cdot \mathrm{DNS}(t) \mid \langle z_{\mathrm{dp}}, z_{\mathrm{rp}}\rangle \, dz_{\mathrm{rp}}\, dz_{\mathrm{dp}}. \tag{14}$$

$\Omega(t)$ can derived through different methods depending on the way the integral in (14) is computed.

1) *Simulation and Fluid-dynamics (SIM-F) method:* The integral in (14) is computed by averaging the values of $\mathrm{DNS}(t) \mid \langle \chi_{\mathrm{dp}}, \chi_{\mathrm{rp}}\rangle$ for a large number of paired samples $\langle \chi_{\mathrm{dp}}, \chi_{\mathrm{rp}}\rangle$ from $f_{\langle \theta_{\mathrm{dp}}, \theta_{\mathrm{rp}}\rangle}$, obtained through stochastic simulation of the procedure model of Fig. 3 according to the dynamic-sTPN semantics illustrated in Section III-A

$$\Omega(t) = \frac{1}{|\mathcal{S}|} \sum_{\langle \chi_{\mathrm{dp}}, \chi_{\mathrm{rp}}\rangle \in \mathcal{S}} \mathrm{DNS}(t) \mid \langle \chi_{\mathrm{dp}}, \chi_{\mathrm{rp}}\rangle \tag{15}$$

where $\mathcal{S}$ is the set of sampled values of $\langle \theta_{\mathrm{dp}}, \theta_{\mathrm{rp}}\rangle$ and $|\mathcal{S}|$ is its cardinality.

2) *Grid Sampling and Fluid-dynamics (GS-F) method:* The integral in (14) is computed by discretization according to the samples of $f_{\langle \theta_{\mathrm{dp}}, \theta_{\mathrm{rp}}\rangle}$ taken over a regular grid Γ, as illustrated in Section III-D

$$\Omega(t) = \sum_{\langle \chi_{\mathrm{dp}}, \chi_{\mathrm{rp}}\rangle \in \Gamma} \gamma_{\langle \chi_{\mathrm{dp}}, \chi_{\mathrm{rp}}\rangle} \big(\mathrm{DNS}(t) \mid \langle \chi_{\mathrm{dp}}, \chi_{\mathrm{rp}}\rangle\big). \tag{16}$$

3) *Grid Sampling and Quick Fluid-dynamics (GS-QF) method:* In the (usual) case in which the impact of the procedure terminates as soon as the WDS topology is restored, i.e., $\mathrm{DNS}(t) \mid \langle \chi_{\mathrm{dp}}, \chi_{\mathrm{rp}}\rangle = 0 \;\; \forall\, t > \chi_{\mathrm{rp}}$, the number of EPANET runs needed to compute the value of $\mathrm{DNS}(t) \mid \langle \chi_{\mathrm{dp}}, \chi_{\mathrm{rp}}\rangle \;\forall \langle \chi_{\mathrm{dp}}, \chi_{\mathrm{rp}}\rangle \in \Gamma$ in (16) can be significantly reduced. In fact, given that the WDS is a physical causal system, its current state does not depend on its future inputs, i.e., $\mathrm{DNS}(t) \mid \langle \chi_{\mathrm{dp}}, \chi_{\mathrm{rp}_1}\rangle = \mathrm{DNS}(t) \mid \langle \chi_{\mathrm{dp}}, \chi_{\mathrm{rp}_2}\rangle \;\; \forall\, t < \min\{\chi_{\mathrm{rp}_1}, \chi_{\mathrm{rp}_2}\}$. According to this, for each $\langle \chi_{\mathrm{dp}}, \chi_{\mathrm{rp}}\rangle \in \Gamma$, the value of $\mathrm{DNS}(t) \mid \langle \chi_{\mathrm{dp}}, \chi_{\mathrm{rp}}\rangle$ can be derived as

$$\mathrm{DNS}(t) \mid \langle \chi_{\mathrm{dp}}, \chi_{\mathrm{rp}}\rangle = \begin{cases} \mathrm{DNS}(t) \mid \langle \chi_{\mathrm{dp}}, \chi^{\max}_{\mathrm{dp,rp}}\rangle & t \le \chi_{\mathrm{rp}} \\ 0 & t > \chi_{\mathrm{rp}} \end{cases} \tag{17}$$

where $\chi^{\max}_{\mathrm{dp,rp}} = \max\{\chi_{\mathrm{rp}} \in \mathbb{R}_{\ge 0} \mid \langle \chi_{\mathrm{dp}}, \chi_{\mathrm{rp}}\rangle \in \Gamma\}$. In doing so, the number of EPANET runs becomes linear in the number of values of θ_{dp} considered in the grid, rather than linear in the number of grid points. The assumption that no lack of service is perceived after pipe reconnection is not proven to hold in principle but is expected to be verified in most real WDSs, and it has been empirically checked on the WDS considered in the experiments.

C. Complexity

The computational complexity of the proposed solution methods depends on the quantitative evaluation of the procedure timing and on the fluid-dynamic analysis of the WDS hybrid behavior. On one hand, stochastic simulation of the procedure model samples $f_{\langle \theta_{\mathrm{dp}}, \theta_{\mathrm{rp}}\rangle}$ by performing a number of steps that is roughly proportional to the number of activities in the model, each step having a linear cost in the number of enabled transitions, which, in turn, can be upper-bounded by the maximum concurrency degree among the model timers. In the (alternative) analytical evaluation of $f_{\langle \theta_{\mathrm{dp}}, \theta_{\mathrm{rp}}\rangle}$, the complexity of the enumeration of the transient tree grows with the overall number of activities, the number of concurrent activities, the length of supports, and the number of time points at which the fluid-dynamic process is affected by maintenance activities, which however is not likely to increase beyond two in a single failure scenario. The subsequent derivation of the symbolic form of $f_{\langle \theta_{\mathrm{dp}}, \theta_{\mathrm{rp}}\rangle}$ has a linear cost in the number of leaf nodes in the transient tree, which in turn depends on the possible different behaviors through which the procedure can be executed; conversely, the cost of sampling $f_{\langle \theta_{\mathrm{dp}}, \theta_{\mathrm{rp}}\rangle}$ over a regular grid is marginal with respect to the computational complexity of the derivation of $f_{\langle \theta_{\mathrm{dp}}, \theta_{\mathrm{rp}}\rangle}$.

On other hand, the gradient solution method used in EPANET needs to invert the Jacobian matrix at each iteration in order to update the solution. If the WDS features M nodes, the size of the matrix is M^2, and the cost of each iteration is estimated to be $O(M^3)$. Desired accuracy also affects the complexity of fluid-dynamic analysis. Once the last calculated solution is in a neighborhood of the real solution, the number of iterations is $O(\log L)$, where L is the desired number of correct digits. However, due to the approximation in input data, the needed accuracy is quite low (a relative error of 10^{-3} is usually accepted) and does not vary sensibly across networks.

Overall, the SIM-F method performs N stochastic simulations of the procedure model to draw N samples from $f_{\langle \theta_{\mathrm{dp}}, \theta_{\mathrm{rp}}\rangle}$, executing an EPANET run for each samples, i.e., N EPANET runs. Both the GS-F method and the GS-QF method draw N samples from $f_{\langle \theta_{\mathrm{dp}}, \theta_{\mathrm{rp}}\rangle}$ by sampling the symbolic form of $f_{\langle \theta_{\mathrm{dp}}, \theta_{\mathrm{rp}}\rangle}$ over a regular grid: while the GS-F method performs N EPANET runs, the GS-QF method permits to reduce the number of EPANET runs to $\sqrt{N}$ in the case that all nodes are served with sufficient pressure as soon as the WDS topology is restored.

V. Computational Experience

We validate the effectiveness of the proposed solution methods on the case of a real WDS with actual load profiles, assessing result accuracy and computational complexity.

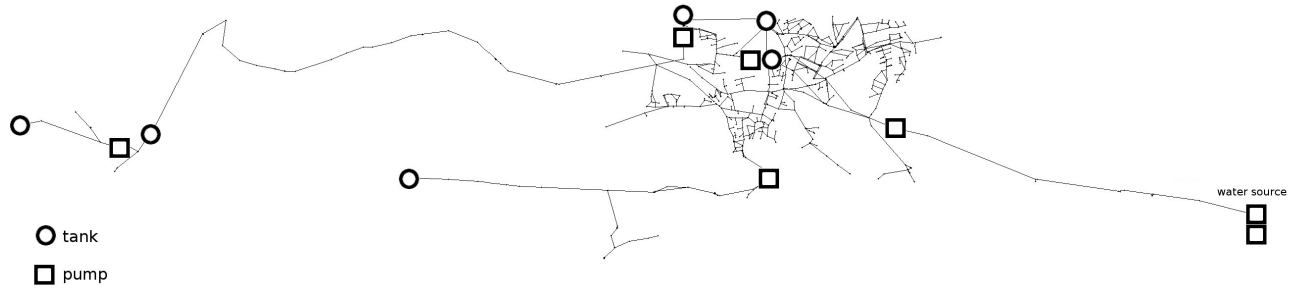

Fig. 5. Schematic of the WDS of the town of Richmond, U.K.

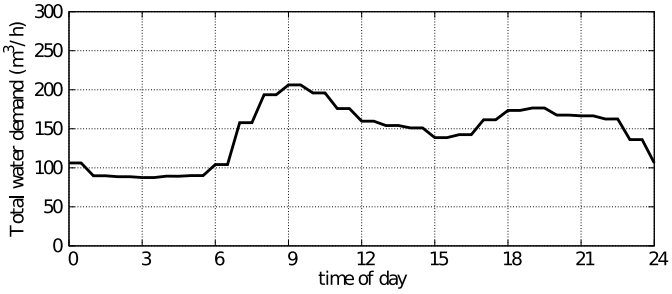

Fig. 6. Total water demand during the day for the WDS shown in Fig. 5.

All the experiments have been performed on a machine equipped with an Intel Xeon 2.67 GHz and 32.0 GB RAM.

A. Real Water Distribution System

We consider the WDS of the town of Richmond [22], [23], U.K., for which most data are made freely available for research purposes by the Yorkshire Water company, including in particular network topology, node heights, and consumption profiles. A schematic of the WDS is shown in Fig. 5, with the source located in the bottom right corner and the highest elevation zone in the top left corner. The WDS model is supplied in the EPANET input format, and consists of 474 load nodes with a peak total demand of 205 m^3/h, 391 junctions, 948 pipes for a total length of 75.6 km, six cascading tanks, seven level-controlled pumps, and one pressure reducing valve. The tanks supply different pressure zones, while all the supplied water is provided in the first place by a treatment plant, modeled as a reservoir, located in the lowest pressure zone. Each tank is fed by a pumping station which is level-controlled, i.e., the corresponding pump(s) is powered when the tank level falls below a given threshold. Each tank supplies its served zone by gravity.

The nodal demand is characterized by 13 different load profiles, most of which feature a lower consumption level during the night hours ([23:00,6:00]) and two peaks of consumption during daytime. The WDS water demand, i.e., the flow rate provided by reservoirs and tanks to the overall WDN, is plotted in Fig. 6, showing two peaks within the time intervals [7:00,10:00] and [16:00,22:00].

B. Experimental Results

1) Estimation of Ground Truth: To evaluate the accuracy of the proposed methods, a *ground truth* is estimated through a very long run of the SIM-F method. To this end, $f_{\langle\theta_{\mathrm{dp}},\theta_{\mathrm{rp}}\rangle}$ (i.e., the joint PDF of the stochastic times when the procedure affects the WDS behavior) is sampled by performing stochastic simulation of the procedure model of Fig. 3 according to the dynamic-sTPN semantics defined in Section III-A. During a simulation run of the procedure model, the PDF of each transition is sampled at newly enabling, using the Metropolis-Hastings algorithm [45], [46] for GEN transitions with a nonuniform distribution. To circumvent the problem of correlated samples, an under-sampling step is derived through the Ljung-Box test [47], which checks the absence of serial correlation up to a given lag. More specifically, for each nonuniform GEN distribution, 10^7 samples are drawn and under-sampled with step $u = 10, 11, \ldots, 150$; then, for each value of u, the Ljung Box test is repeated with lag 1, 2, ..., 10 and significance level 0.01. Experimental results indicate: 1) strong evidence of correlation up to any tested lag for $u \leq 15$ for all the considered distributions (in the majority of cases, the p-value is lower than 10^{-3}); 2) evidence of correlation for $15 < u < 100$ for half of the considered distributions (in several cases, the p-value is lower than or very close to 0.01); and 3) very weak evidence of correlation for $u \geq 100$ for all the considered distributions (only in a very few cases the p-value is lower than 0.01, which can be ascribed to the test uncertainty). According to these results, stochastic simulation can be safely performed using an under-sampling step equal to 100 for any nonuniform GEN transition.

Let $\{\mathcal{S}_i\}_{i\in\mathbb{N}}$ be independent sets of samples with cardinality increasing with i, generated from $f_{\langle\theta_{\mathrm{dp}},\theta_{\mathrm{rp}}\rangle}$ through stochastic simulation of the dynamic-sTPN of Fig. 3, and let $\Omega(t)_{\mathcal{S}_i}$ be the expected DNS over time, computed through the SIM-F approach by solving (15) with the samples in $\mathcal{S}_i$. The Root Mean Square Error (RMSE) is used to measure the difference between the time series values of $\Omega(t)_{\mathcal{S}_i}$ and $\Omega(t)_{\mathcal{S}_j}$ for time values of interest $t = t_1, \ldots, t_N$, and is consistently expressed in the same units as $\Omega(t)$ (m^3/s in SI units)

$$\mathrm{RMSE}(\mathcal{S}_i, \mathcal{S}_j) = \sqrt{\frac{1}{N}\sum_{t=t_1}^{t_N}\left(\Omega(t)_{\mathcal{S}_i} - \Omega(t)_{\mathcal{S}_j}\right)^2}. \qquad (18)$$

TABLE I
ACCURACY AND COMPUTATION TIME OF $\Omega(t)$ COMPUTED BY THE SIM-F METHOD FOR EACH SAMPLE SET $\mathcal{S}_i$

	$\mathcal{S}_1$	$\mathcal{S}_2$	$\mathcal{S}_3$	$\mathcal{S}_4$	$\mathcal{S}_5$	$\mathcal{S}_6$	$\mathcal{S}_7$	$\mathcal{S}_8$	$\mathcal{S}_9$
Number of samples	10^2	$5 \cdot 10^2$	10^3	$5 \cdot 10^3$	10^4	$5 \cdot 10^4$	10^5	$5 \cdot 10^5$	10^6
Time for sample generation	5 s	0.2 min	0.3 min	0.8 min	1.8 min	0.1 h	0.3 h	1.4 h	2.7 h
Time for fluid-dynamic analysis	16 s	1.7 min	2.4 min	11.1 min	21.9 min	2.3 h	5.2 h	17.3 h	49.0 h
Total time	21 s	1.8 min	2.7 min	11.9 min	23.6 min	2.4 h	5.5 h	18.7 h	51.7 h
RMSE$(\mathcal{S}_i, \mathcal{S}_9)$ / m^3h^{-1}	0.0147	0.0113	0.0029	0.0022	0.0020	0.0013	0.0008	0.0002	ref.

A ground truth $\Phi(t)$ for the expected DNS over time $\Omega(t)$ is thus estimated by iteratively computing $\Omega(t)_{\mathcal{S}_i}$ until RMSE$(\mathcal{S}_{i-1}, \mathcal{S}_i)$ is not larger than an assigned threshold ϕ equal to $10^{-5} \cdot \max_{i \in \mathbb{N}}\{\Omega(t)_{\mathcal{S}_i}\}$

$$\Phi(t) \stackrel{\text{def}}{=} \Omega(t)_{\mathcal{S}_G} \quad \text{with } G = \min_{i \in \mathbb{N}, i>1} \{i \mid \text{RMSE}(\mathcal{S}_{i-1}, \mathcal{S}_i) \leq \phi\}. \tag{19}$$

Fig. 7 shows $\Omega(t)_{\mathcal{S}_i}$ computed through the SIM-F method according to independent sets of samples $\mathcal{S}_1$ to $\mathcal{S}_9$ with increasing cardinality (specifically, $|\mathcal{S}_1| = 10^2$, $|\mathcal{S}_2| = 5 \cdot 10^2$, $|\mathcal{S}_3| = 10^3$, $|\mathcal{S}_4| = 5 \cdot 10^3$, $|\mathcal{S}_5| = 10^4$, $|\mathcal{S}_6| = 5 \cdot 10^4$, $|\mathcal{S}_7| = 10^5$, $|\mathcal{S}_8| = 5 \cdot 10^5$, and $|\mathcal{S}_9| = 10^6$). As the number of samples increases, $\Omega(t)_{\mathcal{S}_i}$ almost converges to $\Omega(t)_{\mathcal{S}_9}$, which achieves RMSE$(\mathcal{S}_8, \mathcal{S}_9) \leq \phi$ and is assumed as the ground truth $\Phi(t)$. For any sample set $\mathcal{S}_i$, $\Omega(t)_{\mathcal{S}_i}$ assumes nonnull values over a time interval of three days, roughly following the daily consumption pattern shown in Fig. 6. The peak within [16:00,22:00] is higher on day 1 than on day 2, due to the fact that the peak on day 1 accounts for the DNS when *Reconnect pipe* is completed after 22:00 on day 1, which includes the cases where *Reconnect pipe* is completed after 22:00 on day 2, accounted by the peak on day 2; in a similar manner, the peak within [7:00,10:00] is higher on day 2 than on day 3. No lack of service is experienced in the time range [7:00,10:00] on day 1, given that *disconnect pipe* is never completed before 11:00 on day 1; moreover, no lack of service is visible after 18:00 on day 3 given that the probability that *Reconnect pipe* is executed after that time is nearly lower than 0.00015. Differences between the sample sets are larger for large values of t, because the probability that *Reconnect pipe* is completed after 18:00 on day 3 is nearly 0.624.

Table I shows the values of RMSE$(\mathcal{S}_i, \mathcal{S}_9)$ $\forall\ i = 1, \ldots, 8$ ($\Omega(t)_{\mathcal{S}_9}$ is assumed as the ground truth $\Phi(t)$) and the computational complexity of the evaluation of each $\Omega(t)_{\mathcal{S}_i}$, distinguishing the time spent in sample generation and in fluid-dynamic analysis. As expected, with increasing sample set size, accuracy improves and computation times grow. The RMSE value is reasonably low—around 10^{-3} m^3h^{-1}—when compared to the average value of the measure (see Fig. 7, maximum value around $2.3\,m^3h^{-1}$). Even the roughest model $\mathcal{S}_1$ features an RMSE of less than 1.5%, showing that the overall approach is feasible for the degree of accuracy normally required by the industrial practice in the field. Reducing the error to one tenth requires a 500 times longer computation time, strongly decreasing the convenience of the method.

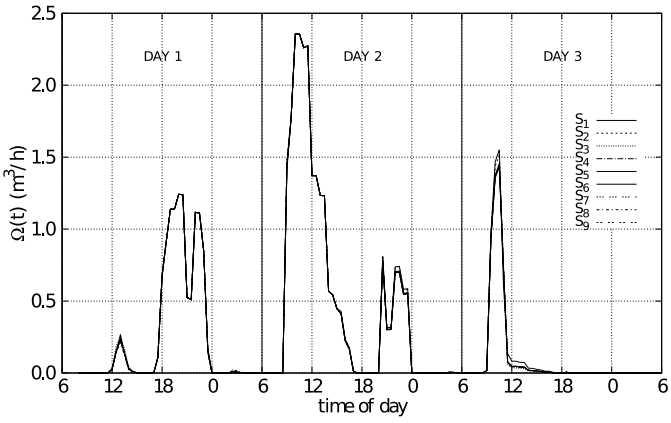

Fig. 7. Expected DNS over time $\Omega(t)_{\mathcal{S}_i}$ computed by the SIM-F method with a time-step of 0.5 h, using independent sets of samples $\mathcal{S}_1$ to $\mathcal{S}_9$ with increasing cardinality, generated from $f_{\langle\theta_{\text{dp}},\theta_{\text{rp}}\rangle}$ by simulation of the dynamic-sTPN model of the procedure shown in Fig. 3.

2) Evaluation of Accuracy and Complexity: We assess the accuracy of the proposed analytical methods against the estimated ground truth $\Phi(t)$. To this end, we compute $\Omega(t)$ according to (16), using sample sets $\{\mathcal{R}_i\}_{i \in \mathbb{N}}$ with increasing cardinality generated by sampling $f_{\langle\theta_{\text{dp}},\theta_{\text{rp}}\rangle}$ (i.e., the joint PDF of the stochastic times when the procedure affects the WDS behavior) over a regular grid, as illustrated in Section III-D. Points on the grid are defined so that

$$\begin{cases} \delta\theta_{\text{dp}} = \dfrac{\theta_{\text{dp}}^{\max} - \theta_{\text{dp}}^{\min}}{N} \\ \delta\theta_{\text{rp}} = \dfrac{\theta_{\text{rp}}^{\max} - \theta_{\text{rp}}^{\min}}{N} \end{cases}$$

where: $\theta_{\text{dp}}^{\min}$ and $\theta_{\text{dp}}^{\max}$ ($\theta_{\text{rp}}^{\min}$ and $\theta_{\text{rp}}^{\max}$) are the minimum and maximum values of θ_{dp} (θ_{rp}), respectively, over the joint support $D_{\langle\theta_{\text{dp}},\theta_{\text{rp}}\rangle}$ of the stochastic times when the procedure affects the WDS behavior, i.e., $\theta_{\text{dp}}^{\min} = 3\,\text{h}$, $\theta_{\text{dp}}^{\max} = 5\,\text{h}$, $\theta_{\text{rp}}^{\min} = 29\,\text{h}$, and $\theta_{\text{rp}}^{\min} = 81.5\,\text{h}$; and, N is equal to 63, 125, 250, and 500 for $\mathcal{R}_1$, $\mathcal{R}_2$, $\mathcal{R}_3$, and $\mathcal{R}_4$, respectively.

Fig. 8 shows $\Omega(t)_{\mathcal{R}_i}$ computed according to $\mathcal{R}_i$ through the GS-F method (curves obtained through the GS-QF method are coincident), whereas Table II shows the number of fluid-dynamic runs through EPANET, the computation times, and the values of RMSE$(\mathcal{R}_i, \mathcal{S}_9)$ for both the GS-F and the GS-QF methods. Note that the time for sample generation and the

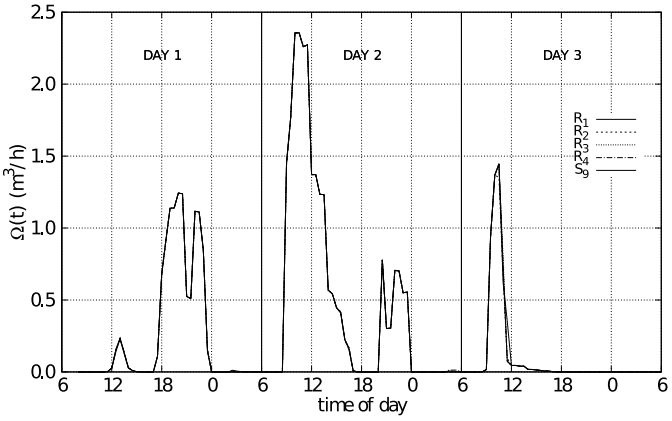

Fig. 8. Expected DNS over time $\Omega(t)_{\mathcal{R}_i}$ computed by the GS-F method with a time-step of 0.5 h, using independent sets of samples $\mathcal{R}_1$ to $\mathcal{R}_4$ with increasing cardinality (curves obtained with the GS-QF method are coincident); the ground truth $\Phi(t) = \Omega(t)_{\mathcal{S}_9}$ is also shown.

TABLE II
ACCURACY AND COMPUTATION TIME OF $\Omega(t)$ COMPUTED BY THE GS-F METHOD AND THE GS-QF METHOD FOR EACH SAMPLE SET $\mathcal{R}_i$

	$\mathcal{R}_1$	$\mathcal{R}_2$	$\mathcal{R}_3$	$\mathcal{R}_4$
Time for sample generation	1.4 min	3.2 min	10.1 min	34.4 min
GS-F METHOD				
No. fluid-dynamics runs	1694	6365	22 290	84 118
Time for fluid-dynamics	4.1 min	15.8 min	0.9 h	3.7 h
Total time	5.4 min	19.0 min	1.1 h	4.3 h
RMSE / m^3h^{-1}	0.0206	0.0081	0.0053	0.0015
GS-QF METHOD				
No. fluid-dynamics runs	64	126	251	501
Time for fluid-dynamics	0.6 min	1.9 min	5.7 min	20.7 min
Total time	2.0 min	5.1 min	15.8 min	55.1 min
RMSE / m^3h^{-1}	0.0216	0.0078	0.0053	0.0014

accuracy are the same for both methods, whereas they differ in terms of number of and time spent in fluid-dynamic analyses. As expected, Table II shows that the number of fluid-dynamic analyses is much lower for the GS-QF method, given that only one run for each value of θ_{dp} in the sample set is performed. This leads to a great improvement in total computation times, which range from 5.4 min to 4.3 h for the GS-F method and from 2.0 to 55.1 min for the GS-QF method, the convenience of the GS-QF method being greater for the grids featuring finer granularity. Both methods feature similar values of RMSE, the small differences being ascribed to numerical errors in the sum of a great number of small probabilities.

VI. DISCUSSION

WDSs are a class of hybrid systems with a continuous dynamics determined by a number of variables such as tank levels, demand patterns, and discrete states of components like valves and pumps. Given a network topology, a control policy for discrete state components, and nodal demand patterns, the evolution over time of pressure and service quality is determined and can be efficiently computed through the EPANET tool. However, during maintenance operations–quite frequent in the practice either for contingencies or for planned interventions—network topology is changed at stochastic time points corresponding to the completion of repair phases. This casts the problem of performability evaluation of the impact of a maintenance procedure into the class of SHSs, for which existing general numerical or simulative solution techniques cannot afford the complexity of realistic WDSs.

As far as we know, we propose the first approach allowing the quantitative evaluation of the DNS over time in a WDS subject to a phased maintenance procedure with stochastic durations; the advancement of the approach is also emphasized by the ability to encompass random durations beyond the limits of a Markovian setting, and suspension of activities during nonworking hours. The problem is formulated as an analysis of performability conditional to the occurrence of an incident, which makes the approach independent from failure probabilities of components. The solution process decouples stochastic evaluation of the procedure timing from hybrid analysis of the WDS subordinated to each procedure phase, sampling the joint distribution of the time points when the network topology is affected by maintenance activities, either by stochastic simulation of the procedure model (SIM-F method) or by symbolic analysis based on an extension of the method of stochastic state classes (GS-F method). Performability measures are then obtained by executing EPANET fluid-dynamic analysis for each sample and weighting the results according to sample probabilities. If the WDS can be assumed not to suffer any lack of service after the normal network topology is restored, as expected in most WDSs and empirically verified for the studied WDS, a single fluid-dynamic analysis provides the results for multiple timing values, and computation times can be significantly reduced (GS-QF method) by changing the order of magnitude of the number of repetitions of fluid dynamic analysis.

Experimental results show that, when a coarse-grained accuracy is sufficient—not lower than 1% in the studied WDS—and thus a small number of samples is enough, the simulative SIM-F method attains the best tradeoff between accuracy and efficiency, which may become even more relevant if the complexity of the maintenance procedure grows. On the other hand, the computation time of the analytical GS-F and GS-QF methods grows more slowly with the number of samples and is less sensitive to the contribution of fluid-dynamic calculation cost, so that this becomes the best solution when a higher degree of accuracy is needed–lower than 0.1% for the studied WDS–or when more complex WDS models are considered.

Experimental evaluation on a real WDS shows that the proposed approach is feasible, with an accuracy of 1% attained in nearly 20 s and an accuracy of 0.1% attained in nearly 55 min. Moreover, there is still substantial room for improvement in the enhancing of several toolchain details such as file I/O and sorting. Thanks to the mild level of complexity and the independence from failure probabilities of components, an exploitation of the proposed technique in higher level analyses can be envisaged, especially when repeated evaluation is

required under some iteration of procedure parameters. From a tactical perspective, the approach might offer support when optimizing the schedule of multiple maintenance interventions, helping to select a convenient start time and to inform users regarding the expected extent of lack of service. Conversely, from a strategic perspective, the proposed solution could drive the collection of quantitative data for the estimation of stochastic parameters of repair procedures. Additional benefits could also arise in the validation and improvement of maintenance strategies, in the allocation of budget for network strengthening policies, and in multiobjective optimization supporting robust WDS design.

The current major hurdle to the complete application of the proposed approach is the availability of accurate statistical data on repair durations. Actually, the growing spread of smart devices is facilitating the collection of such data, which is likely to be available to WDS operators in the near future. Notably, the availability of failure probabilities on various classes of components (e.g., by age, material, depth, surface traffic, parasitic currents, etc.) would pave the way to leveraging the approach in a probabilistic failure modes and effects analysis, as a support to risk assessment and early identification of critical failure scenarios. Moreover, the proposed approach could also serve as the basis for further solution techniques addressing multiple failures and disaster recovery, which present major challenges to cope with the larger number of stochastic time points at which maintenance affects the WDS behavior.

APPENDIX

We extend the calculus of stochastic state classes [20] according to the dynamic-sTPN semantics of Section III-A, encompassing clock valuations, fickle functions, and marking-dependent CDFs. To maintain the joint domain of $\vec{\tau}$, τ_{age}, and $\vec{\nu}$ in DBM form, τ_{age} and $\vec{\nu}$ encode the opposite of the elapsed time and the opposite of the clock values, respectively.

Let $\Sigma = \langle m, D_{\langle\vec{\tau},\tau_{\text{age}},\vec{\nu}\rangle}, f_{\langle\vec{\tau},\tau_{\text{age}},\vec{\nu}\rangle}\rangle$ be a class with $\langle\vec{\tau},\tau_{\text{age}},\vec{\nu}\rangle = \langle\tau_1,\ldots,\tau_N,\tau_{\text{age}},\nu_1,\ldots,\nu_M\rangle$. Transition t_1 turns out to be firable in Σ iff: 1) $D_a = D_{\langle\vec{\tau},\tau_{\text{age}},\vec{\nu}\rangle} \cap \{x_1 \le x_i \ \forall\ i = 2,\ldots,N\}$ is not empty and 2) the firing probability $\mu_1 = \int_{D_a} f_{\langle\vec{\tau},\tau_{\text{age}},\vec{\nu}\rangle}(\vec{x}, x_{\text{age}}, \vec{y})\, d\vec{x}\, dx_{\text{age}}\, d\vec{y}$ is greater than zero, with $\vec{x} = \langle x_1,\ldots,x_N\rangle$ and $\vec{y} = \langle y_1,\ldots,y_M\rangle$. The successor $\Sigma' = \langle m', D'_{\langle\vec{\tau}',\tau'_{\text{age}},\vec{\nu}'\rangle}, f'_{\langle\vec{\tau}',\tau'_{\text{age}},\vec{\nu}'\rangle}\rangle$ of Σ through t_1 with probability μ_1 is derived through the following steps.

1) *Conditioning:* The assumption that t_1 fires conditions $\langle\vec{\tau},\tau_{\text{age}},\vec{\nu}\rangle$ and yields a new random vector $\langle\vec{\tau}^a,\tau^a_{\text{age}},\vec{\nu}^a\rangle = \langle\vec{\tau},\tau_{\text{age}},\vec{\nu}\rangle \mid \tau_1 \le \tau_i\ \forall\ i = 2,\ldots,N$, distributed over D_a according to the following PDF:

$$f_{\langle\vec{\tau}^a,\tau^a_{\text{age}},\vec{\nu}^a\rangle}\left(\vec{x}, x_{\text{age}}, \vec{y}\right) = \frac{f_{\langle\vec{\tau},\tau_{\text{age}},\vec{\nu}\rangle}\left(\vec{x}, x_{\text{age}}, \vec{y}\right)}{\mu_1}. \quad (20)$$

2) *Time Advancement and Projection:* The firing of t_1 reduces each timer by τ_1^a and eliminates τ_1^a by a projection, yielding the random vector $\langle\vec{\tau}^b,\tau^b_{\text{age}},\vec{\nu}^b\rangle = \langle\tau_2^a-\tau_1^a,\ldots,\tau_N^a-\tau_1^a,\tau^a_{\text{age}}-\tau_1^a,\nu_1^a-\tau_1^a,\ldots,\nu_M^a-\tau_1^a\rangle$, distributed over the projection $D_a \downarrow x_1$ of D_a that eliminates τ_1^a, i.e., $D_a \downarrow x_1 \coloneqq \{\langle\vec{x}, x_{\text{age}}, \vec{y}\rangle \mid \exists\ x_1 \in \mathbb{R}_{\ge 0}$ s.t. $\langle x_1,\vec{x}, x_{\text{age}}, \vec{y}\rangle \in D_a\}$ with $\vec{x} = \langle x_2,\ldots,x_N\rangle$, according to the following PDF:

$$f_{\langle\vec{\tau}^b,\tau^b_{\text{age}},\vec{\nu}^b\rangle}\left(\vec{x}, x_{\text{age}}, \vec{y}\right) = \int_{\min_1(\vec{x},x_{\text{age}},\vec{y})}^{\max_1(\vec{x},x_{\text{age}},\vec{y})} f_{\langle\vec{\tau}^a,\tau^a_{\text{age}},\vec{\nu}^a\rangle}\left(x_1, \vec{x}+x_1, x_{\text{age}}+x_1, \vec{y}+x_1\right) \cdot dx_1 \quad (21)$$

where $\vec{x} + x_1 = \langle x_2 + x_1,\ldots,x_N + x_1\rangle$, $\vec{y} + x_1 = \langle y_1 + x_1,\ldots,y_M + x_1\rangle$, and $\min_1(\vec{x}, x_{\text{age}}, \vec{y})$ and $\max_1(\vec{x}, x_{\text{age}}, \vec{y})$ are the minimum and the maximum values of x_1 s.t. $\langle x_1, \vec{x}+x_1, x_{\text{age}}+x_1, \vec{y}+x_1\rangle \in D_a$, respectively. To simplify notation, let $D_b = D_a \downarrow x_1$. Moreover, the time-to-fire of each transition t_i s.t. $I(t_i)(m', t_1) = \delta_i \ne 0$ is increased by the deterministic value δ_i, e.g., if $I(t_2)(m', t_1) = \delta_2 \ne 0$, we get a new random vector $\langle\vec{\tau}^c,\tau^c_{\text{age}},\vec{\nu}^c\rangle = \langle\tau_2^b+\delta_2,\ \tau_3^b,\ldots,\tau_N^b,\tau^b_{\text{age}},\nu_1^b,\ldots,\nu_M^b\rangle$ distributed over $D_c = \{\langle x_2,\vec{x},\vec{y}\rangle \mid \langle x_2-\delta_2,\vec{x},\vec{y}\rangle \in D_b\}$, with $\vec{x} = \langle x_3,\ldots,x_N\rangle$, according to the following PDF:

$$f_{\langle\vec{\tau}^c,\tau^c_{\text{age}},\vec{\nu}^c\rangle}\left(\vec{x}, x_{\text{age}}, \vec{y}\right) = f_{\langle\vec{\tau}^b,\tau^b_{\text{age}},\vec{\nu}^b\rangle}\left(x_2-\delta_2, \vec{x}, x_{\text{age}}, \vec{y}\right). \quad (22)$$

3) *Disabling:* The time-to-fires of the transitions disabled by the firing of t_1 and the valuations of clocks in $Y(t_1)$ are eliminated through a projection, e.g., if t_2 is disabled and $\nu_1 \in Y(t_1)$, we get a new random vector $\langle\vec{\tau}^d,\tau^d_{\text{age}},\vec{\nu}^d\rangle = \langle\tau_3^c,\ldots,\tau_N^c,\tau^c_{\text{age}},\nu_2^c,\ldots,\nu_M^c\rangle$ with support $D_d = D_c \downarrow x_2 \downarrow y_1$ and the following PDF:

$$f_{\langle\vec{\tau}^d,\tau^d_{\text{age}},\vec{\nu}^d\rangle}\left(\vec{x}, x_{\text{age}}, \vec{y}\right) = \int_{\min_1^{\nu}(\vec{x},x_{\text{age}},\vec{y})}^{\max_1^{\nu}(\vec{x},x_{\text{age}},\vec{y})} \int_{\min_2(\vec{x},x_{\text{age}},y_1,\vec{y})}^{\max_2(\vec{x},x_{\text{age}},y_1,\vec{y})} f_{\langle\vec{\tau}^c,\tau^c_{\text{age}},\vec{\nu}^c\rangle}\left(x_2,\vec{x},x_{\text{age}},y_1,\vec{y}\right) dx_2\, dy_1 \quad (23)$$

where $\vec{x} = \langle x_3,\ldots,x_N\rangle$; $\vec{y} = \langle y_2,\ldots,y_M\rangle$; $\min_2(\vec{x}, x_{\text{age}}, y_1, \vec{y})$ and $\max_2(\vec{x}, x_{\text{age}}, y_1, \vec{y})$ are the minimum and the maximum values of x_2 such that $\langle x_2,\vec{x},x_{\text{age}},y_1,\vec{y},\rangle \in D_c$, respectively; and, $\min_1^{\nu}(\vec{x}, x_{\text{age}}, \vec{y})$ and $\max_1^{\nu}(\vec{x}, x_{\text{age}}, \vec{y})$ are the minimum and the maximum values of y_1 such that $\langle\vec{x}, x_{\text{age}}, y_1, \vec{y},\rangle \in D_c \downarrow x_2$, respectively.

4) *Newly Enabling:* The random vector $\langle\vec{\tau}^d,\tau^d_{\text{age}},\vec{\nu}^d\rangle$ is augmented with the time-to-fire of each transition newly enabled by the firing of t_1 and with the valuation v_i of each clock $c_i \in Y(t_1)$, e.g., if t_{N+1} is newly enabled and $\nu_1 \in Y(t_1)$, we obtain a new random vector $\langle\vec{\tau}',\tau'_{\text{age}},\vec{\nu}'\rangle = \langle\tau_3^d,\ldots,\tau_N^d,\tau_{N+1},\tau_{\text{age}},\nu_1,\nu_2^d,\ldots,\nu_M^d\rangle$ distributed over $D'_{\langle\vec{\tau}',\tau'_{\text{age}},\vec{\nu}'\rangle} = D_d \times [EFT_{t_{N+1},m'}, LFT_{t_{N+1},m'}] \times [0,0]$

according to the following PDF:

$$f'_{\langle \vec{\tau}', \tau'_{\text{age}}, \vec{\nu}' \rangle}\left(\vec{x}, x_{N+1}, x_{\text{age}}, \vec{y}\right) = f_{\langle \vec{\tau}^d, \tau^d_{\text{age}}, \vec{\nu}^c \rangle}\left(\vec{x}, x_{\text{age}}, \vec{y}\right) \cdot f_{t_{N+1}, m'}(x_{N+1}) \cdot \delta(y_1) \tag{24}$$

where $\vec{x} = \langle x_3, \ldots, x_N, x_{N+1} \rangle$ and $\vec{y} = \langle y_1, \ldots, y_M \rangle$.

ACKNOWLEDGMENT

The authors would like to thank the Yorkshire Water company for making the network topology data available.

REFERENCES

[1] H. Methods *et al.*, *Advanced Water Distribution Modeling and Management*. Waterbury, CT, USA: Haestad Press, 2003.
[2] W. Zhao, T. H. Beach, and Y. Rezgui, "Optimization of potable water distribution and wastewater collection networks: A systematic review and future research directions," *IEEE Trans. Syst., Man, Cybern., Syst.*, vol. 46, no. 5, pp. 659–681, May 2016.
[3] J. Lygeros and M. Prandini, "Stochastic hybrid systems: A powerful framework for complex, large scale applications," *Eur. J. Control*, vol. 16, no. 6, pp. 583–594, 2010.
[4] A. Abate, J.-P. Katoen, J. Lygeros, and M. Prandini, "Approximate model checking of stochastic hybrid systems," *Eur. J. Control*, vol. 16, no. 6, pp. 624–641, 2010.
[5] M. H. A. Davis, "Piecewise-deterministic Markov processes: A general class of non-diffusion stochastic models," *J. Roy. Stat. Soc. B (Methodol.)*, vol. 46, no. 3, pp. 353–388, 1984.
[6] M. L. Bujorianu and J. Lygeros, "General stochastic hybrid systems: Modelling and optimal control," in *Proc. IEEE Conf. Decis. Control*, 2004, pp. 1872–1877.
[7] H. A. P. Blom and E. A. Bloem, "Exact Bayesian and particle filtering of stochastic hybrid systems," *IEEE Trans. Aerosp. Electron. Syst.*, vol. 43, no. 1, pp. 55–70, Jan. 2007.
[8] Z. Ding, Y. Zhou, M. Jiang, and M. Zhou, "A new class of Petri nets for modeling and property verification of switched stochastic systems," *IEEE Trans. Syst., Man, Cybern., Syst.*, vol. 45, no. 7, pp. 1087–1100, Jul. 2015.
[9] X. D. Koutsoukos and D. Riley, "Computational methods for verification of stochastic hybrid systems," *IEEE Trans. Syst., Man, Cybern. A, Syst., Humans*, vol. 38, no. 2, pp. 385–396, Mar. 2008.
[10] K. S. Trivedi and V. G. Kulkarni, "FSPNs: Fluid stochastic Petri nets," in *Application and Theory of Petri Nets 1993* (LNCS 691), M. A. Marsan, Ed. Berlin, Germany: Springer, 1993, pp. 24–31.
[11] G. Horton, V. G. Kulkarni, D. M. Nicol, and K. S. Trivedi, "Fluid stochastic Petri nets: Theory, applications, and solution techniques," *Eur. J. Oper. Res.*, vol. 105, no. 1, pp. 184–201, 1998.
[12] M. Gribaudo and A. Horvath, "Fluid stochastic Petri nets augmented with flush-out arcs: A transient analysis technique," *IEEE Trans. Softw. Eng.*, vol. 28, no. 10, pp. 944–955, Oct. 2002.
[13] K. Wolter, G. Horton, and R. German, "Non-Markovian fluid stochastic Petri nets," Tech. Univ. at Berlin, Berlin, Germany, Rep. 1996-13, 1996. [Online]. Available: https://pdfs.semanticscholar.org/5faf/a372198e083daeb42bab7809bb20b14b9ccc.pdf
[14] G. Ciardo, D. M. Nicol, and K. S. Trivedi, "Discrete-event simulation of fluid stochastic Petri nets," *IEEE Trans. Softw. Eng.*, vol. 25, no. 2, pp. 207–217, Mar./Apr. 1999.
[15] H. Ghasemieh, A. Remke, B. Haverkort, and M. Gribaudo, "Region-based analysis of hybrid Petri nets with a single general one-shot transition," in *Proc. Int. Conf. Formal Model. Anal. Timed Syst.*, vol. 7595. London, U.K., 2012, pp. 139–154, doi: 10.1007/978-3-642-33365-1_11.
[16] H. Ghasemieh, A. Remke, and B. R. Haverkort, "Analysis of a sewage treatment facility using hybrid Petri nets," in *Proc. Int. Conf. Perform. Eval. Methodol. Tools (ValueTools)*, 2013, pp. 165–174.
[17] H. Ghasemieh, A. Remke, and B. R. Haverkort, "Survivability analysis of a sewage treatment facility using hybrid Petri nets," *Perform. Eval.*, vol. 97, pp. 36–56, Mar. 2016.
[18] C. R. Vázquez and M. Silva, "Stochastic hybrid approximations of Markovian Petri nets," *IEEE Trans. Syst., Man, Cybern., Syst.*, vol. 45, no. 9, pp. 1231–1244, Sep. 2015.
[19] L. Carnevali, M. Paolieri, F. Tarani, and E. Vicario, "Quantitative evaluation of availability measures of gas distribution networks," in *Proc. Int. Conf. Perform. Eval. Method Tools*, 2013, pp. 145–154.
[20] A. Horváth, M. Paolieri, L. Ridi, and E. Vicario, "Transient analysis of non-Markovian models using stochastic state classes," *Perf. Eval.*, vol. 69, nos. 7–8, pp. 315–335, 2012.
[21] E. Vicario, L. Sassoli, and L. Carnevali, "Using stochastic state classes in quantitative evaluation of dense-time reactive systems," *IEEE Trans. Softw. Eng.*, vol. 35, no. 5, pp. 703–719, Sep./Oct. 2009.
[22] J. E. Van Zyl, D. A. Savic, and G. A. Walters, "Operational optimization of water distribution systems using a hybrid genetic algorithm," *J. Water Resources Plan. Manag.*, vol. 130, no. 2, pp. 160–170, 2004.
[23] M. López-Ibáñez, T. D. Prasad, and B. Paechter, "Ant colony optimization for optimal control of pumps in water distribution networks," *J. Water Resources Plan. Manag.*, vol. 134, no. 4, pp. 337–346, 2008.
[24] P. Pratheeba, "Optimization for maintenance of water distribution system using stochastic search algorithms," M.S. thesis, Faculty Civil Eng., Anna Univ., Chennai, India, 2013.
[25] American Water Works Association, *New or Repaired Water Mains*, United States Environ. Protect. Agency, Washington, DC, USA, 2002.
[26] *Water Safety in Distribution Systems*, document WHO/FWC/WSH/14.03, WHO Document Product. Services, World Health Org., Geneva, Switzerland, 2014.
[27] *Technical Notes on Drinking-Water, Sanitation and Hygiene in Emergencies*, Water Eng. Develop. Centre, World Health Org., Geneva, Switzerland, 2013.
[28] T. M. Walski and A. Pelliccia, "Economic analysis of water main breaks," *J. Amer. Water Works Assoc.*, vol. 74, no. 3, pp. 140–147, 1982.
[29] M. Tabesh, J. Soltani, R. Farmani, and D. Savic, "Assessing pipe failure rate and mechanical reliability of water distribution networks using data-driven modeling," *J. Hydroinformat.*, vol. 11, no. 1, pp. 1–17, 2009.
[30] D. Shinstine, I. Ahmed, and K. Lansey, "Reliability/availability analysis of municipal water distribution networks: Case studies," *J. Water Resources Plan. Manag.*, vol. 128, no. 2, pp. 140–151, 2002.
[31] J. M. Wagner, U. Shamir, and D. H. Marks, "Water distribution reliability: Simulation methods," *J. Water Resources Plan. Manag.*, vol. 114, no. 3, pp. 276–294, 1988.
[32] G. Darvini, P. Salandin, and L. Da Deppo, "Coping with uncertainty in the reliability evaluation of water distribution systems," in *Proc. Annu. Water Distrib. Syst. Anal. Conf. (WDSA)*, 2008, pp. 483–498.
[33] B. Zhuang, K. Lansey, and D. Kang, "Reliability/availability analysis of water distribution systems considering adaptive pump operation," in *Proc. World Environ. Water Resources Congr.*, 2011, pp. 224–233.
[34] "The water distribution code," Abu Dhabi Distrib. Company, East Lansing, MI, USA, Rep. 3.0, Jul. 2010.
[35] A. Bobbio, A. Puliafito, and M. Telek, "A modeling framework to implement preemption policies in non-Markovian SPNs," *IEEE Trans. Softw. Eng.*, vol. 26, no. 1, pp. 36–54, Jan. 2000.
[36] G. Ciardo, A. Blakemore, P. Chimento, J. Muppala, and K. Trivedi, *Automated Generation and Analysis of Markov Reward Models Using Stochastic Reward Nets* (IMA Volumes in Mathematics and Its Applications), vol. 48. New York, NY, USA: Springer, 1993, pp. 145–191.
[37] B. Berthomieu, S. Dal Zilio, L. Fronc, and F. Vernadat, "Time Petri nets with dynamic firing dates: Semantics and applications," in *Proc. Int. Conf. Formal Model. Anal. Timed Syst.*, 2014, pp. 85–99.
[38] L. Carnevali, L. Grassi, and E. Vicario, "State-density functions over DBM domains in the analysis of non-Markovian models," *IEEE Trans. Softw. Eng.*, vol. 35, no. 2, pp. 178–194, Mar./Apr. 2009.
[39] ORIS Tool. (2016). *Homepage*. [Online]. Available: http://www.oris-tool.org
[40] "Bentley water distribution software updates," *World Pumps*, vol. 2014, no. 11, p. 11, 2014, doi: 10.1016/S0262-1762(14)70267-6.
[41] KyPipes. (2016). *Homepage*. [Online]. Available: http://kypipe.com/kypipe
[42] WatDis. (2016). *Homepage*. [Online]. Available: http://www.watdis.com
[43] EPANET. (2016). *Homepage*. [Online]. Available: http://www.epa.gov/water-research/epanet
[44] H. Alegre, *Performance Indicators for Water Supply Services*. London, U.K.: IWA, 2006.
[45] N. Metropolis, A. W. Rosenbluth, M. N. Rosenbluth, A. H. Teller, and E. Teller, "Equation of state calculations by fast computing machines," *J. Chem. Phys.*, vol. 21, no. 6, pp. 1087–1092, Jun. 1953.

[46] W. K. Hastings, "Monte Carlo sampling methods using Markov chains and their applications," *Biometrika*, vol. 57, no. 1, pp. 97–109, Apr. 1970.
[47] G. M. Ljung and G. E. P. Box, "On a measure of lack of fit in time series models," *Biometrika*, vol. 65, no. 2, pp. 297–303, 1978.

Laura Carnevali received the B.S. and M.S. degrees in informatics engineering and the Ph.D. degree in informatics, multimedia, and telecommunications engineering from the University of Florence, Florence, Italy, in 2004, 2006, and 2010, respectively.

She is an Assistant Professor of Computer Science (with a tenure track) with the School of Engineering, University of Florence. Her current research interest includes correctness verification and performance evaluation of real-time systems, with specific interest on stochastic characterization of timed models.

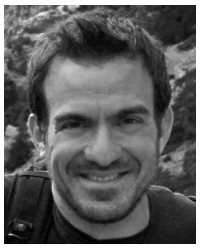

Fabio Tarani received the B.S. degree in mechanical engineering, and the M.S. and Ph.D. degrees in energy engineering from the University of Florence, Florence, Italy, in 2005, 2008, and 2012, respectively.

He is a Temporary Research Fellow with the School of Engineering, University of Florence. His current research interests include the design and optimization of energy systems, with a special focus on renewable sources, and of energy/power distribution networks and grids, to the energy assessment of buildings.

Enrico Vicario (M'95) received the M.S. degree in electronics engineering and the Ph.D. degree in informatics and telecommunications engineering from the University of Florence, Florence, Italy, in 1990 and 1994, respectively.

He is a Full Professor of Computer Science and the Head of the Information Engineering Department, University of Florence. His current research interests include model-based approaches for development, verification, and quantitative evaluation of concurrent systems with nondeterministic and stochastic temporal parameters.